

Tectonics

RESEARCH ARTICLE

10.1029/2018TC005153

Key Points:

- Paleomagnetic data reveal mean, thrust-scale rotations ranging from 0 to +38° in the Central Axial Zone
- We interpret vertical-axis rotations in terms of basement thrust kinematics
- New constraints on the 3-D geometry of the Pyrenean Axial Zone are derived

Supporting Information:

- Supporting Information S1

Correspondence to:

E. Izquierdo-Llavall,
 eizquierdollavall@gmail.com

Citation:

Izquierdo-Llavall, E., Casas-Sainz, A. M., Oliva-Urcia, B., Villalaín, J. J., Pueyo, E., & Scholger, R. (2018). Rotational kinematics of basement antiformal stacks: Paleomagnetic study of the western Nogueras zone (central Pyrenees). *Tectonics*, 37, 3456–3478. <https://doi.org/10.1029/2018TC005153>

Received 7 JUN 2018

Accepted 2 SEP 2018

Accepted article online 5 SEP 2018

Published online 3 OCT 2018

©2018. American Geophysical Union.
 All Rights Reserved.

Rotational Kinematics of Basement Antiformal Stacks: Paleomagnetic Study of the Western Nogueras Zone (Central Pyrenees)

Esther Izquierdo-Llavall¹ , Antonio M. Casas-Sainz^{2,3} , Belén Oliva-Urcia⁴ , Juan J. Villalaín⁵ , Emilio Pueyo^{3,6}, and Robert Scholger⁷ 

¹E2S-UPPA, UPPA-CNRS-Total, Laboratoire des Fluides Complexes et leurs Réservoirs, IPRA, Université de Pau et des Pays de l'Adour, Pau, France, ²Departamento de Ciencias de la Tierra, Universidad de Zaragoza, Zaragoza, Spain, ³Unidad Asociada en Ciencias de la Tierra IGME/Universidad de Zaragoza, Universidad de Zaragoza, Zaragoza, Spain, ⁴Departamento de Geología y Geoquímica, Universidad Autónoma de Madrid, Madrid, Spain, ⁵Departamento de Física, Universidad de Burgos, Burgos, Spain, ⁶Instituto Geológico y Minero de España, Unidad de Zaragoza, Zaragoza, Spain, ⁷Chair of Applied Geophysics, University of Leoben, Leoben, Austria

Abstract The structure of the Pyrenean Axial Zone laterally transitions from an imbricate thrust system to an antiformal stack displaying downward facing structures in its frontal part (the Nogueras zone). We carried out a paleomagnetic study through this structural transition to better constrain thrust kinematics and better define the factors controlling the occurrence of antiformal stacks. Triassic red beds unconformably overlying the Paleozoic basement were sampled across three main thrust sheets (the Nogueras zone, the Bielsa, and the Orri thrust sheets). From 31 new sites, two meaningful magnetizations were defined, both carried by hematite: (1) the primary magnetization, that unblocks at 660–685 °C and (2) an intermediate-temperature, syn-orogenic remagnetization. Paleomagnetic data indicate variable, clockwise vertical axis rotations, with mean, thrust-scale values that range from 0 to +38°. They increase both from the base to the top of the stacked units and from west to east and display a thrust-scale directional dispersion that is higher for the lower wavelength thrusts. Results evidence that increasing thrust displacements in the upper thrusts units are a key factor for the formation of antiformal stacks showing downward facing structures. Displacement gradients in the basement are transferred to cover units and can account for important rotations such as those registered by the Mesozoic-Cenozoic units to the south of the study area.

1. Introduction

Basement antiformal stacks are common in the inner, Axial Zone of orogens such as the Bohemian massif (Zulauf & Duyster, 1997), the Sevier orogenic belt (DeCelles et al., 1995), or the central Pyrenees (Muñoz, 1992). They result from the vertical stacking of thrust sheets that produces an overall antiformal geometry with the frontal part of the upper thrusts being forward rotated (Figures 1a and 1b, schematic sections B and C). The along-strike variation in the displacement (Figure 1a) and/or number (Figure 1b) of thrusts in a fold-and-thrust system may produce its lateral change from an antiformal stack to an imbricate thrust system (Figures 1a and 1b, schematic sections A). The latter is characterized by thrust surfaces that always dip toward the hinterland, with thrust units displaying a degree of vertical overlap that is lower than in antiformal stacks. Assuming a piggyback thrust sequence, two end-members can be schematically depicted to explain such variation: (i) the presence of a constant number of thrust sheets with the upper units displaying lateral displacement changes (Figure 1a) or (ii) the along-strike change in the number of thrust sheets, the higher thrust number yielding the stronger vertical stacking (Figure 1b).

The study of these lateral variations can be undertaken through the determination of vertical axis rotations (VARs) by means of paleomagnetic methods (Allerton, 1998; Dinarès et al., 1992; McCaig & McClelland, 1992; McClelland & McCaig, 1989a, 1989b; Sussman & Weil, 2004; Weil & Sussman, 2004). In the first kinematic scenario (Figure 1a), we could expect that along-strike displacement gradients are resolved through VARs in the upper thrust units whereas the lower thrust sheets remain unrotated. On the contrary, in the second scenario, local VARs could occur in the lateral termination of the lower thrust units, affecting older thrust sheets

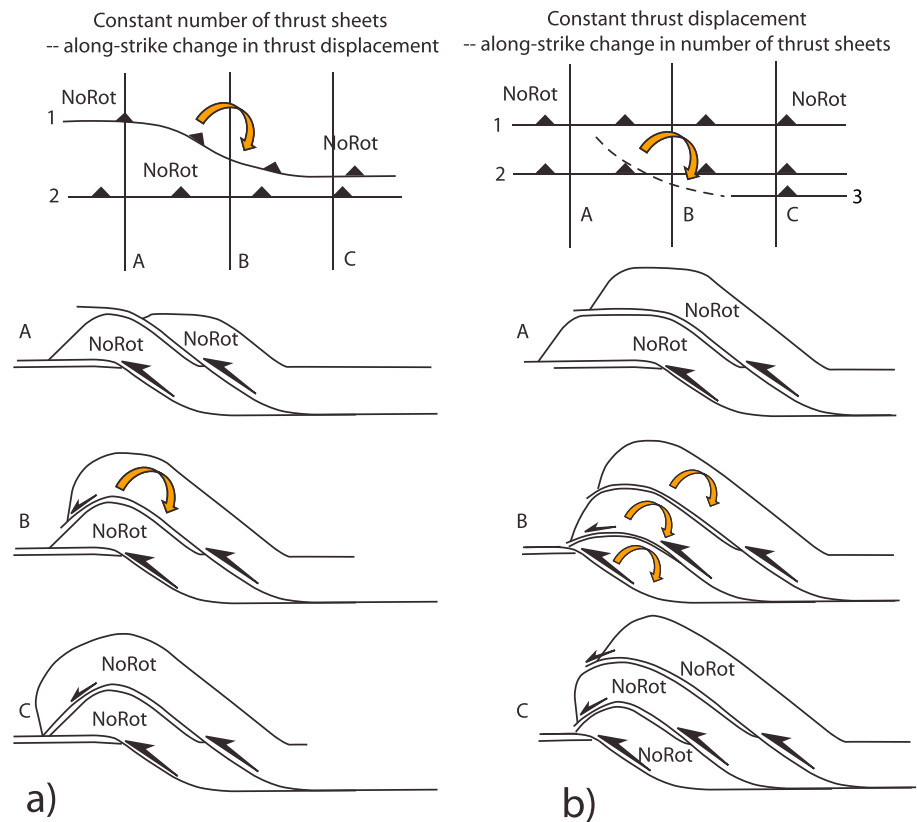


Figure 1. End-member models explaining the lateral change from an antiformal stack to an imbricate thrust system in a piggyback thrust sequence. Sense (clockwise in all cases) and distribution of the expected VARs is indicated. VARs = vertical axis rotations. NoRot refers to unrotated domains/thrust units.

in their hanging wall. Intermediate stages would involve a mixture of processes and related VARs. Besides, these rotations can affect the overlying units, and thus, rotated domains can expand across the strike of fold-and-thrust systems.

The Pyrenean Axial Zone represents an excellent laboratory for the investigation of the factors controlling along-strike variations in basement thrust stacks as well as their interaction with cover units. Basement thrusting in the Axial Zone began during Late Cretaceous times (Muñoz, 2002), coevally to the onset of the collision between the Iberian and European proximal margins (Mouthereau et al., 2014). Thrusting mostly took place in a piggyback thrust sequence with the last faulting stages being accomplished during the Early Miocene (Teixell, 1998). The Axial Zone is formed by Paleozoic units unconformably overlain by Lower-Middle Triassic and Upper Cretaceous sequences (Figure 2). In the central Pyrenees, the Axial Zone is represented by an asymmetric, south verging antiformal stack, characterized by a strong vertical overlap of thrust units, the uppermost one (the Nogueras unit) being forward rotated (Muñoz, 1992; Figure 2c). Conversely, to the west, the thrust wedge forming the Axial Zone becomes wider: thrust sheets display a lower overlap, and downward facing structures are not found (Martínez-Peña & Casas-Sainz, 2003; Teixell, 1996, Figure 2b). Preserved, foreland-dipping thrusts end laterally up along the Ésera valley (see location in Figures 2 and 3a) that is besides located to the NE of the strongly rotated cover units in the western South Pyrenean Central Unit (SPCU in Figure 2; VARs up to +50–70°, Dinarès-Turell, 1992; Fernández, 2004; Garcés et al., 2016; Mochales et al., 2012; Muñoz et al., 2013; Pueyo, 2000; Rodríguez-Pintó et al., 2016).

The structural transition occurring in this domain is of potential interest to investigate rotational kinematics in basement thrust systems that change along strike. With this aim, we carried out a paleomagnetic study of the Lower-Middle Triassic units in the different basement thrusts that crop out in the area (the Nogueras, Bielsa, and Orri thrust sheets; see cross sections in Figures 3b and 3c).

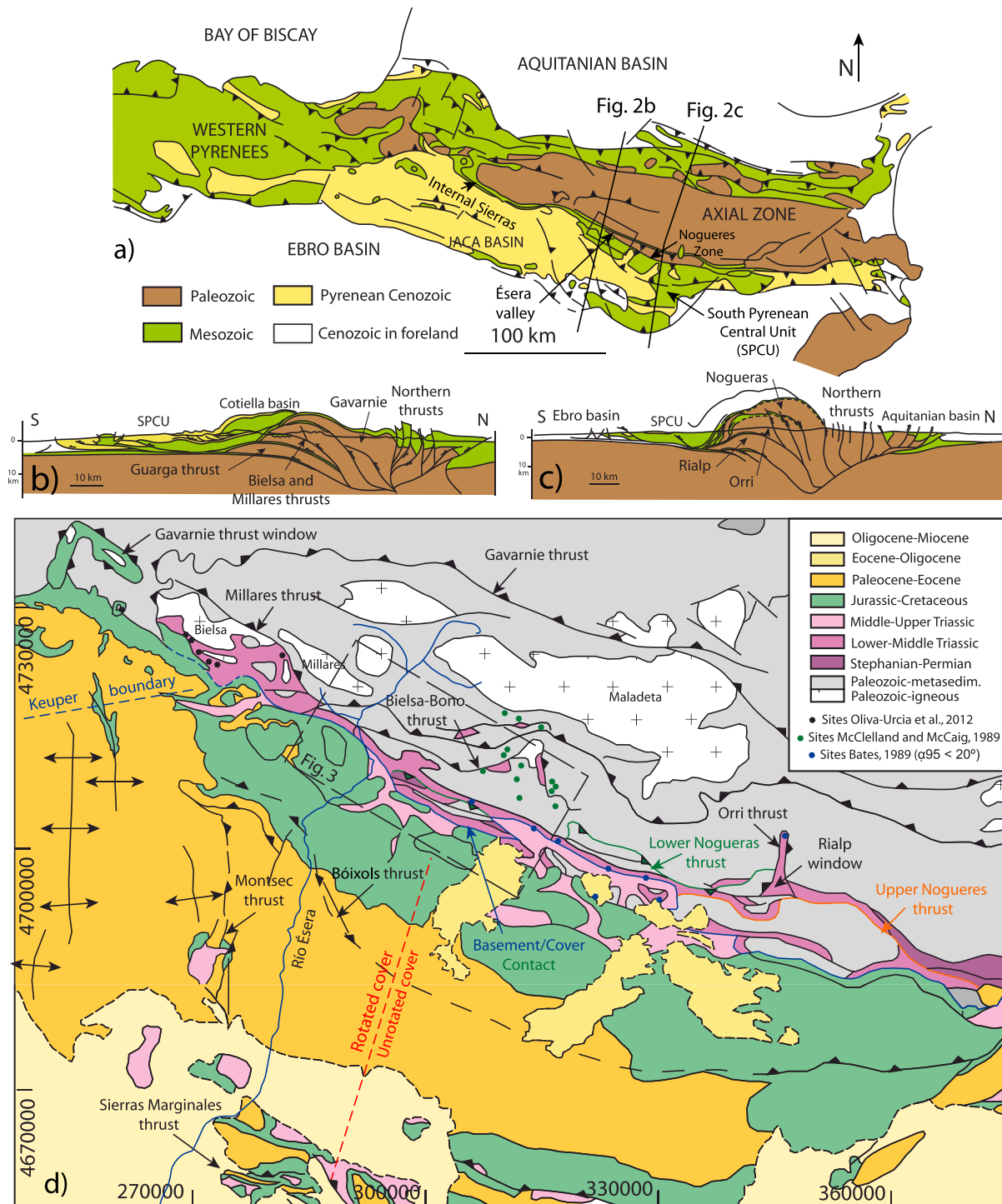


Figure 2. (a) Geological map of the Pyrenees showing the location of the study area (modified from Teixell, 1998). Range-scale cross sections modified from (b) Martínez-Peña and Casas-Sainz (2003) and (c) Muñoz (1992). Their location is indicated in Figure 2a. Notice the along-strike change in the number of basement thrust sheets and the geometry of the basement thrust system. (d) Geological map of the south-central Axial Zone and the Nogueras Zone (modified from Barnolas et al., 2008, universal transverse mercator (UTM) coordinates, 31 T). Location of previous paleomagnetic sites in basement units is indicated. The Nogueras Zone is divided into the lower and upper Nogueras thrust sheets (based on Muñoz, 1992; ICGC, 2014). The dashed, red line in the SPCU separates rotated cover units to the west from unrotated Mesozoic-Cenozoic sequences to the east, whereas the dashed blue line marks the boundary of the Keuper evaporites (from Muñoz et al., 2013). SPCU = South Pyrenean Central Unit.

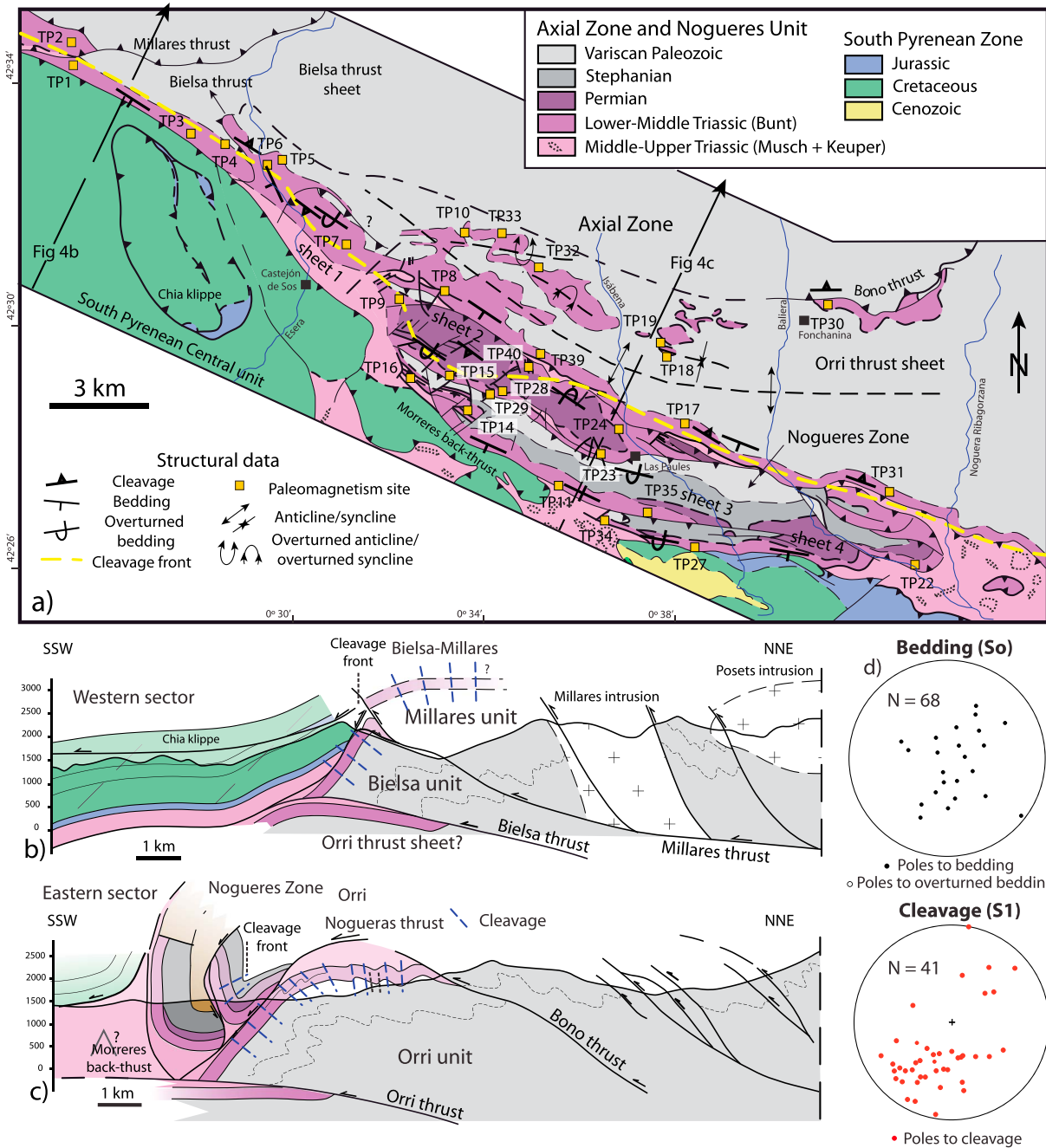


Figure 3. Geological map of the study area (modified from Mey, 1968 and Wennekers, 1968) including location of the paleomagnetic sites and the cross sections in Figures 3b and 3c. Mapping in the area of transition between the Nogueras Zone and the Bielsa-Bono and Orri thrust sheets was modified with respect to the original geological mapping (see Izquierdo-Llavall, Casas-Sainz, et al., 2013, where an additional downward facing anticline was mapped in the western Nogueras Zone, immediately to the east of an oblique thrust ramp located below the Bielsa thrust surface, probably approaching the western termination of the Orri thrust). Cross sections across the western (b) and the eastern (c) part of the study area (Izquierdo-Llavall, Casas-Sainz, et al., 2013). They extend to the north of the map in Figure 3a (see Figure 2d). (d) Equal-area plots show the orientation of the poles to bedding (So) and cleavage (S1) for the whole study area.

The paleomagnetic data reported constitute a new data set that allows quantification of the absolute VARs throughout the studied thrust sheets. These data are compared to previous rotation values obtained in basement units to the east and west of the study area (Bates, 1989; McClelland & McCaig, 1989a, 1989b; Olivarcia et al., 2012) to obtain a broader picture of the 3-D distribution of basement rotations and to evaluate

their contribution to (i) the development and along-strike change in the Axial Zone and (ii) the strong rotations registered by the cover units of the western SPCU.

2. Geological Setting

2.1. Stratigraphic Setting

The Axial Zone is formed, in the study area, by sedimentary and low-grade metamorphic rocks of Silurian to Carboniferous age unconformably overlain by Stephanian, Permian, and Triassic rocks (Zwart, 1979). Silurian to Carboniferous units were deformed during the Variscan Orogeny (Middle-Late Carboniferous; García-Sanseguno, 1996; Poblet, 1991). During the late-Variscan stages (Stephanian to Permian), sedimentation took place in small, fault-bounded basins (Gisbert, 1983; Gisbert et al., 1985; Saura & Teixell, 2006) with important volcanic activity (Martí & Mitjavila, 1987) that were subsequently overlain by extensive Triassic sequences showing the typical *Germanic* facies: Buntsandstein red beds, Muschelkalk limestones, and Keuper evaporites and shales. The Buntsandstein starts with a basal conglomerate followed by interbedded sandstones and shales and has an average thickness of 200 m (García Senz et al., 2009, Figure 3a). The Muschelkalk limestones occur as discontinuous outcrops within the Keuper (Mey, 1968; Wennekers, 1968) that is strongly deformed because it acted as a major décollement during the Alpine Orogeny (Late Cretaceous-Cenozoic).

To the south of the Triassic units (Figure 3a), thick sequences of Jurassic to Oligocene units crop out (SPCU, Figure 2). The Jurassic and Lower Cretaceous units are mainly formed by marine sequences (Caus et al., 1990), whereas Upper Cretaceous to Oligocene units are mostly syn-contractual and registered an evolution from marine to transitional and finally continental environments (Puigdefàbregas et al., 1992). Thick sequences of conglomerates were deposited during late Lutetian to late Oligocene times (Beamud et al., 2011, Figure 2d).

2.2. Structural Setting: The Axial Zone

2.2.1. Basement Deformation

The main Alpine structures in the study area are the basement thrusts forming the Axial Zone thrust system, with a floor thrust within the Paleozoic units and a roof thrust in the Upper Triassic, Keuper layers. Taking into account the range-scale geometry of the Axial Zone, the studied area is located at the transition between two different along-strike structural domains (Figure 2a). In the western domain, the thrust system forming the Axial Zone includes four main basement thrust sheets, from the base to the top, the Guarga, Bielsa, Millares, and Gavarnie thrusts (Figures 2b, 3b, Martínez-Peña & Casas-Sainz, 2003; Román-Berdiel et al., 2004, 2006). They are hinterland dipping and form a thrust system displaying a moderate vertical stacking of basement units. Two of the thrust sheets forming this system crop out in the sampled area, Millares and Bielsa. The latter involves Lower-Middle Triassic red beds in its hanging wall, describing a wide, fault bend anticline geometry (Figure 3b). In the eastern domain, the Axial Zone is formed by three main basement thrust sheets (Muñoz, 1992; Figure 2c), from the base to the top: the Rialp, Orri, and Nogueras thrusts. They form an antiformal stack, the upper thrusts displaying downward facing folds along its frontal part (Nogueras Zone). The Orri thrust sheet (Muñoz, 1992) groups three south directed thrusts (note that taking into account this observation, the total number of basement thrust sheets increases from the western to the eastern domain). Among them, the lower thrust unit (the Orri thrust s.s. and hereinafter the Orri thrust) contains large outcrops of Triassic red beds deformed by an E-W trending hanging wall anticline (Figure 3c, García-Sanseguno, 1996; Gutiérrez-Medina, 2007; Poblet, 1991). To the south of this anticline, the Nogueras Zone involves (in the study area) Permian red beds, Stephanian volcanics, and Paleozoic units of Orri affinity (Muñoz, 1992) and consists of four foreland-dipping thrust slices (sheets 1 to 4 in Figure 3a) that are related to forelandward-rotated synformal anticlines (the so-called *têtes-plongeantes*, Séguret, 1972). Based on Muñoz (1992) and Institut Cartogràfic i Geològic de Catalunya (ICGC, 2014), these thrust units belong to the lower Nogueras unit.

The lateral connection between basement thrusts in the western (Figure 3b) and eastern sectors (Figure 3c) of the study area is hindered by the discontinuity of Triassic outcrops lying on the basement and by the complex structure affecting the Paleozoic units, partly Alpine and partly inherited from Variscan times. Taking into account the structural and geological mapping data, the Orri thrust sheet has been interpreted to end laterally along the Ésera Valley (Izquierdo-Llavall, Casas-Sainz, et al., 2013). Its emplacement contributed to the westward tilting of the Bielsa thrust surface that is below the topographic surface to the west but crops

out to the east of the study area, probably connecting to the Bono thrust (see location in Figure 3a; hereinafter the surface comprising these two thrusts is called Bielsa-Bono thrust).

Alpine thrusting in the Axial Zone was accompanied by folding and cleavage development (Izquierdo-Llavall, Aldega, et al., 2013; see location of the cleavage front in Figure 3a). Cleavage in the Triassic units is pervasive to the north (Orri and Bielsa-Bono thrust units; Figure 3a) but disappears toward the southerner thrust sheets of the Nogueras Zone (thrust sheets 3 and 4 in Figure 3a). It is ESE-WNW striking (subparallel to the strike of bedding) and axial planar (Figure 3d, Izquierdo-Llavall, Casas-Sainz, et al., 2013; Séguret, 1972). Previous magnetic fabrics (anisotropy of magnetic susceptibility) data in the Triassic units of the study area (Izquierdo-Llavall, Casas-Sainz, et al., 2013) indicate a heterogeneous distribution of deformation that is in agreement with the distribution of cleavage.

2.2.2. Deformation in the Cover Units

Shortening in the basement of the Axial Zone was transferred to cover units (Upper Triassic to Cenozoic) where the large imbricate thrust system of the SPCU developed. Cover and basement thrust systems are separated by a complex passive backthrust (Morreres backthrust, Muñoz, 1992; Figures 2d and 3a). South of the studied area, the SPCU is formed by an arcuate fold-and-thrust system detached in the Upper Triassic evaporites (Keuper unit). It consists of three main thrust units (from the top to the base of the thrust system, the Bóixols, Montsec, and Sierras Marginales thrusts, see Figure 2d) that (i) were emplaced in a piggy-back thrust sequence, from Late Cretaceous to Oligocene times and (ii) underwent strong clockwise VARs in their westernmost sector reaching maximum values of 50° to 70° (Dinarès-Turell, 1992; Garcés et al., 2016; Mochales et al., 2012; Muñoz et al., 2013, and references therein).

3. Methodology

3.1. Sampling Sites

Thirty-one new paleomagnetic sites were collected from the Lower-Middle Triassic units (Buntsandstein fine-grained sandstones and shales) using a portable water-cooled drill. Each site consists of 9–10 standard paleomagnetic cores distributed in about 3 to 20 m of the stratigraphic succession. Sites were collected throughout the three main basement thrust sheets previously described: Bielsa-Bono (4 sites), Nogueras (15 sites), and Orri (12 sites; Table 1).

Conglomerates interbedded within sandstones were sampled in both the Nogueras and Orri units to perform conglomerate tests. Moreover, fold and tilt tests were applied at local (sites TP18 and TP19) and regional scales.

3.2. Laboratory Procedures

Stepwise thermal demagnetization of the natural remanent magnetization (NRM) was performed at the Gams Paleomagnetic Laboratory (Leoben University, Austria). Magnetization was measured using a 2G DC squid magnetometer (model 760–3.0), and a MMTD oven was used to thermally demagnetize the samples at steps ranging from 5° to 200 °C up to a maximum temperature of 690 °C. Susceptibility was measured during demagnetization using a Bartington MS2 susceptibility meter. Alternating field (AF) pilot demagnetizations were carried out in selected samples using a 2G AF demagnetizer, in field steps ranging from 3 to 10 mT up to a maximum field of 100 mT. AF demagnetization was unable to unravel the NRM and thus not used to determine the Characteristic Remanent Magnetization in this study.

Paleomagnetic components were analyzed using the principal component analysis method and site means were computed using Fisher (1953) statistics. In both cases, the routine provided by the software Remasoft (Chadima & Hrouda, 2006) was used. The virtual directions method and VPD software were also used to calculate site mean directions (Ramón et al., 2017). The statistical confidence of the fold test was determined by McFadden and Jones (1981) and Tauxe et al. (2010) methods, whereas reversal and inclination-only tests were conducted using the McFadden and McElhinny (1990) and the McFadden and Reid (1982) methods, respectively. To determine the carriers of the magnetization, isothermal remanent magnetization (IRM) acquisition curves (Dunlop, 1972), combined with thermal demagnetization of composite IRM (1.5, 0.4, and 0.12 T fields; Lowrie, 1990), were conducted using a 2G pulse magnetizer model 660 (maximum field of 2.5 T). The IRM acquisition curves (conducted on 10 selected samples that include the different lithological types and the whole range of NRM values) were analyzed by means of the IRM-CLG 1.0 worksheet (Kruiver et al., 2001), which allows the quantification of the mean coercivity values and the relative contribution to

Table 1
New Paleomagnetic Sites in the Southern Axial Zone

Site	Latitude (N)	Longitude (E)	Thrust sheet	Mean NRM intensity (mA/m)	St. dev. NRM	Mean km (10^{-6} S.I.)	St. dev. km
TP1	42°34'10.5"	0°23'57.7"	Bielsa	1.63	0.59	55	9.2
TP2	42°34'25.2"	0°23'52.9"	Bielsa	1.95	0.74	138	45.1
TP3	42° 33' 5.8"	0°26'28.2"	Bielsa	2.08	0.87	136	24.5
TP4	42°33'4.9"	0°27'15.3"	Bielsa	2.85	1.2	114	13.6
TP5	42°32'50.4"	0°28'29.7"	Orri	3.66	0.21	147	10.5
TP6	42°32'42.8"	0°28'06.2"	Orri	1.44	0.52	146	14.9
TP7	42°31'15.7"	0°29'48.8"	Nogueras	4.02	3.26	100	14
TP8	42°30'48.3"	0°31'47.9"	Orri	3.35	1.96	127	17.3
TP9	42°30'42.8"	0°30'57.6"	Nogueras	1.39	1.19	189	21.9
TP10-m	42°31'44.7"	0°32'13.8"	Orri	2.74	0.95	95	19.9
TP10-c	42°31'44.7"	0°32'13.8"	Orri	0.41	0.16	—	—
TP11	42°27'48.4"	0°34'18.6"	Nogueras	3.49	2.08	162	53.1
TP14	42°28'55.4"	0°32'22"	Nogueras	1.51	0.29	78	12.4
TP15	42°29'29.2"	0°31'43.9"	Nogueras	3.22	1.17	221	17.3
TP16	42°29'22"	0°31'10"	Nogueras	1.29	0.43	128	22.5
TP17	42°28'45.1"	0°36'51.2"	Orri	2.11	1.35	149	49.9
TP18	42°30'2.3"	0°36'25.8"	Orri	4.31	2.10	122	39.5
TP19	42° 30' 5.4"	0°36'23.6"	Orri	4.93	1.12	161	11.2
TP22	42°26'35.3"	0°41'46.1"	Nogueras	2.57	1.04	149	45.9
TP23	42°28'18.3"	0°35'7.7"	Nogueras	1.56	0.23	158	43.8
TP24	42°28'42.6"	0°35'29.7"	Nogueras	3.61	1.93	88	21.7
TP27	42°26'44.2"	0°37'11.7"	Nogueras	1.02	0.34	113	18.3
TP28-m	42°29'14"	0°32'58.3"	Nogueras	1.5	1.99	36	10.4
TP28-c	42°29'14"	0°32'58.3"	Nogueras	0.61	0.41	17	23.5
TP29	42°29'0.3"	0°32'55.1"	Nogueras	3.1	1.66	209	59.5
TP30	42°30'51.6"	0°40'07.0"	Orri	3.84	1.34	132	55
TP31	42°27'47.3"	0°41'13.2"	Orri	2.28	1.08	202	25.7
TP32	42°31'14.4"	0°33'50.3"	Orri	2.82	1.30	106	42.6
TP33	42°31'41.2"	0°33'3.1"	Orri	2.67	0.53	93	11.3
TP34	42°27'13.8"	0°35'09.1"	Nogueras	1.64	0.39	136	8.8
TP35	42°27'24.2"	0°36'04"	Nogueras	3.71	0.83	197	14.6
TP39	42°29'48.1"	0°33'47.2"	Orri	2.46	0.54	174	21.9
TP40	42°29'37.9"	0°33'32.8"	Nogueras	5.68	1.61	84	9.4

Note. Name of the site (for location in map view see Figure 3a); latitude and longitude of the site in geographic coordinates (Datum: WGS84); structural location (thrust sheet); site mean Natural Remanent Magnetization (NRM) intensity (in mA/m), and bulk magnetic susceptibility (km) (S.I. units). Standard deviations (St. dev.) are shown for both values. Sites TP10 and TP28 were used to carry out conglomerate tests; matrix (m) and clasts (c) were sampled.

the IRM of the different components. Thermal demagnetization of composite IRM was performed on one sample per site.

4. Paleomagnetic Data

4.1. Magnetic Mineralogy

IRM curves are homogeneous for the different lithological types sampled in the study area (Figures 4a–4f). They show the presence of a hard magnetic carrier that contributes 96 to 99% of the IRM and prevents the complete saturation of the curves at peak fields of 2.5 T.

Thermal demagnetization of the composite IRM (Lowrie, 1990; Figures 4g–4i) shows a strong magnetization of the hard and intermediate axis (1.5 and 0.4 T) and two main, sharp intensity decays between 500 and 630 °C and 660 and 690 °C, suggesting the presence of two hematite phases with slightly different unblocking temperature ranges.

The imperceptible decay of the soft component (120 mT) at ~580 °C demonstrates that the contribution of magnetite is negligible, as also suggested by the inability of AF demagnetization to destroy the NRM

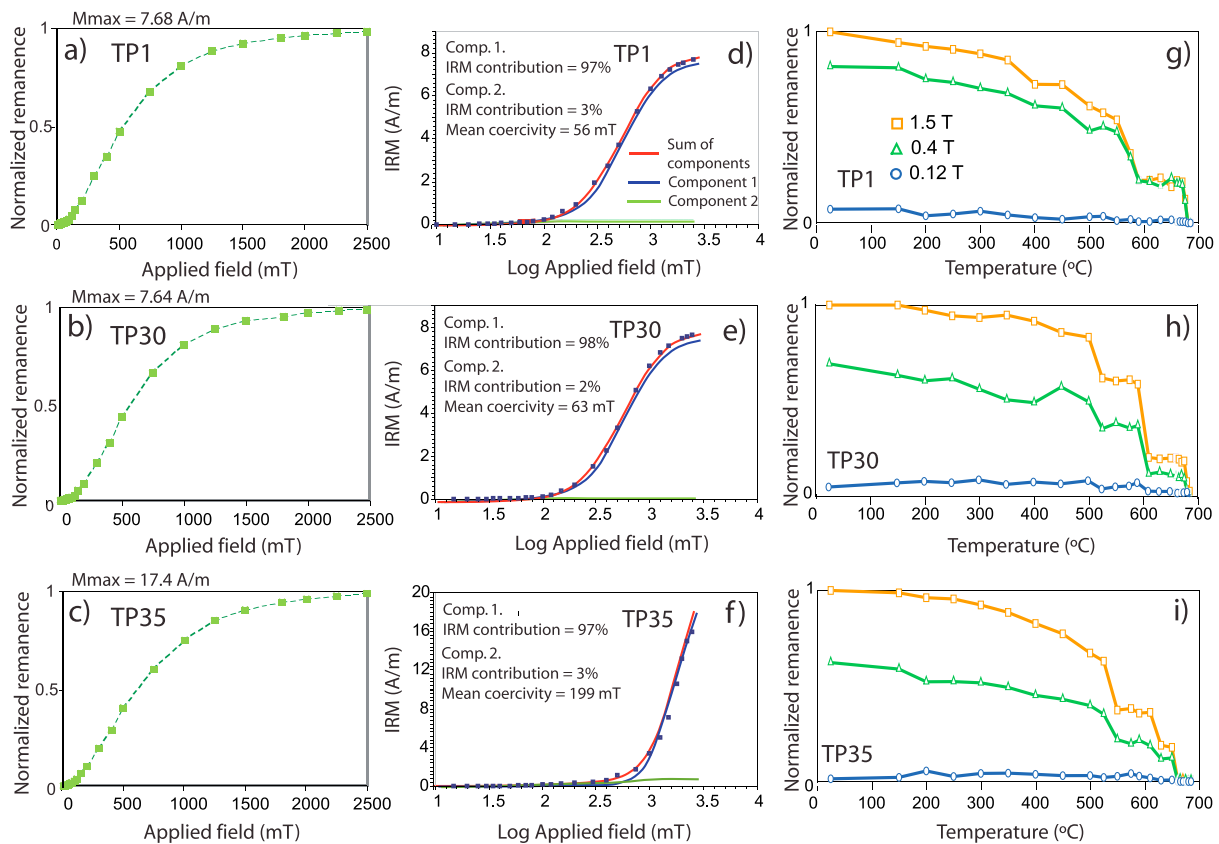


Figure 4. (a–c) Acquisition of the isothermal remanent magnetization (IRM) from representative samples. (d–f) Analysis of the IRM acquisition curves by means of the IRM-CLG 1.0 worksheet (Kruiver et al., 2001). For each component, the percentage of relative contribution to the IRM is shown. (g–i) Stepwise thermal demagnetization of the composite IRM (Lowrie, 1990) for the same samples as in Figures 4a–4c.

(a maximum of the 10%, 19%, and 22% of the magnetization was removed after applying AF fields of 20, 30, and 50 mT, respectively).

4.2. Paleomagnetic Components

Stepwise thermal demagnetization reveals the presence of two stable paleomagnetic components. They consist of a higher-temperature component (C in Table 2; named as C_b, C_o, and C_n in the Bielsa, Orri, and Nogueras units respectively) and an intermediate temperature component (B in Table 2) that occur simultaneously in 58% of sites. In spite of the overlapping observed in several samples, both components were in general successfully isolated.

The C component shows a narrow unblocking temperature interval, ranging from temperatures higher than 650 °C and below 690 °C, and occurs in 74% of the sites (Table 2 and Figure 5), locally showing dual polarity. The B component displays a wider range of unblocking temperatures, from 300–400 to 660 °C (stronger intensity decay usually from 550 °C), and a single polarity at any one site (Table 2). This component has been isolated in 81% of the sites and, in general terms, shows a larger dispersion at the site scale than component C. The observed unblocking temperatures are consistent with the magnetic mineralogy experiments (note the similarity of unblocking temperatures in thermal demagnetizations of both the NRM and the composite IRM) and the AF results and evidence that hematite is the carrier of both C and B paleomagnetic components that were distinguishable by their unblocking temperatures range. Similar results were obtained by Bates (1989) who characterized these two components at similar temperature intervals but did not find the site-scale dual polarity in the high temperature one.

Both components show a strong dispersion in geographic coordinates. After tectonic correction, the clustering of component C improves (suggesting an early acquisition with regard to folding, Figure 6a), whereas

Table 2
Paleomagnetic Data for Components C (Cb in Bielsa, Cn in Nogueras, and Co in Orri thrust sheet) and B

Site	Comp.	n/N	D (BTC)	I (BTC)	α_{95}	k	So-strike	So-dip	D (ATC)	I (ATC)	Polarity
COMPONENT C											
<i>Bielsa thrust sheet</i>											
TP1	Cb	9/9	348	-9.5	14	14	127	55S	341	26	9N/OR
TP3	Cb	8/9	340	-72	11	26	105	90	4	15	8N/OR
<i>Nogueras thrust sheet</i>											
TP7	Cn	7/10	88	59	11	29	130	35N(o)	193	-31	0N/7R
TP24	Cn	8/9	198.5	33	11	28	124	47S(o)	47	13	8N/OR
TP40	Cn	9/9	200	46	13	16	117	59S(o)	32	12	9N/OR
TP9	Cn	10/10	47	57	10	26	120	24N(o)	199	-33	0N/10R
TP15	Cn	10/10	271.5	-32	13	15	130	40N(o)	358	4	10N/OR
TP23	Cn	5/9	200	-35	8	94.5	70	30N(o)	21	11 ^a	3N/2R
TP29	Cn	7/9	173	-36	9.5	41	155	56N(o)	43	7 ^a	7N/OR
TP11	Cn	10/10	309	-72	9	29	110	88S	3	4	5N/5R
TP16	Cn	3/10	256	-48	20	38	135	47N(o)	24	5	3N/OR
TP35	Cn	4/9	71	47	17	29	114	62N(o)	174	4	0N/4R
TP27	Cn	5/10	297	58	30	7	90/70	75N(o)	208	0.5	1N/4R
TP34	Cn	5/9	48	-87	12	40	142	77S	52	-10	5N/OR
<i>Orri thrust sheet</i>											
TP10	Co	5/5	358	23	16	25	80	7S	358	30	5N/OR
TP18	Co	9/10	343	40	7	56	110	12/30N	349	25	9N/OR
TP19	Co	10/10	348	6	4.5	117	105	27S	343.5	30	10N/OR
TP30	Co	4/9	330	42	8.5	118	45	45N	326	-2	4N/OR
TP32	Co	9/10	310	-38	13	16	112	85N(o)	330	17	9N/OR
TP33	Co	9/9	16	18	10.5	25	138	35S	1	46	9N/OR
TP17	Co	5/9	342	-17	20	15	110	41S	342	16	3N/2R
TP31	Co	7/9	5	-6	14	20	115	44/58S	358	42	7N/OR
TP39	Co	7/9	357	-39.5	15.5	16	125	64S	5	15.5	7N/OR
COMPONENT B											
<i>Bielsa thrust sheet</i>											
TP2	B	4/9	355	41	27.5	12	74	50S	87	81	N
TP3	B	7/9	30	-62	9	43	105	90	23	27	N
TP4	B	9/9	331	-77	12	19	115	65N(o)	13	32	N
<i>Nogueras thrust sheet</i>											
Thrust sheets 1-2											
TP7	B	8/10	182	-0.5	17	12	130	35N(o)	83	-26	R
TP9	B	7/10	256	-54	14	21	120	24N(o)	359	35	N
TP15	B	8/10	307	-24	15	14	130	40N(o)	328.5	16.5	N
TP23	B	9/9	170	44	18	9	70	30N(o)	314	-73	R
TP29	B	5/9	130	-43	17	20	155	56N(o)	124	39	R
TP40	B	9/9	204	59	16	11	117	59S(o)	29	0	R
TP24	B	9/9	188	24	22	6	124	47S(o)	59	19	R
TP22	B	8/9	195	71	7	69	090	60N(o)	187.5	-48	R
Thrust sheets 3-4											
TP11	B	8/10	341	27	13	20	110	88S	253	45	N
TP14	B	7/9	334	30	10.5	34	130	36S	309	37	N
TP35	B	9/9	15	-30	7.5	48	114	62N(o)	308.5	82	N
TP27	B	8/10	301	58	17	11	90/70	75N(o)	204	2	N
TP34	B	6/9	12	17	21.5	11	142	77S	311	51	N
<i>Orri thrust sheet</i>											
TP5	B	7/10	66	-55	13	21	114	85S	48	20	N
TP6	B	9/10	131	-11	19	8	27	23W	131	11.5	N
TP18	B	5/10	359	56	13.5	33	110	12/30N	5.5	38	N
TP19	B	6/10	3	25	14	23	105	27S	357	51	N
TP10	B	5/5	3	20	16	24	80	7S	4	27	N
TP30	B	6/9	191	-3.5	18	15	45	45N	197	21	N
TP33	B	8/9	42.5	38	9	40	138	35S	34	72	N
TP8	B	8/10	48	3	20	9	118	51S	59	50	N
TP17	B	8/9	2	-8	14	17	110	41S	359	31	N

Note. Considered paleomagnetic component (Comp.), n/N, number of samples used to calculate the mean (n) from the total number of demagnetized standard samples (N); D and I (BTC), declination and inclination before tectonic correction; α_{95} and k, statistical parameters for a fisherian distribution; So-strike, So-dip, bedding plane (strike and dip) (o) overturned beds; D and I (ATC), declination and inclination after tectonic correction; polarity (N, normal, R, reverse) after bedding correction (component C), or at the inferred remagnetization time (Component B, see supporting information).

^aIn sites TP23 and TP29 bedding planes are oblique to the main N110°E Pyrenean direction. This obliquity is interpreted as due to a precompressional tilting of the beds, and a two-step bedding correction was applied: (i) restoration of Pyrenean folding and (ii) backtilting of the resulting bedding plane after the fold restoration.

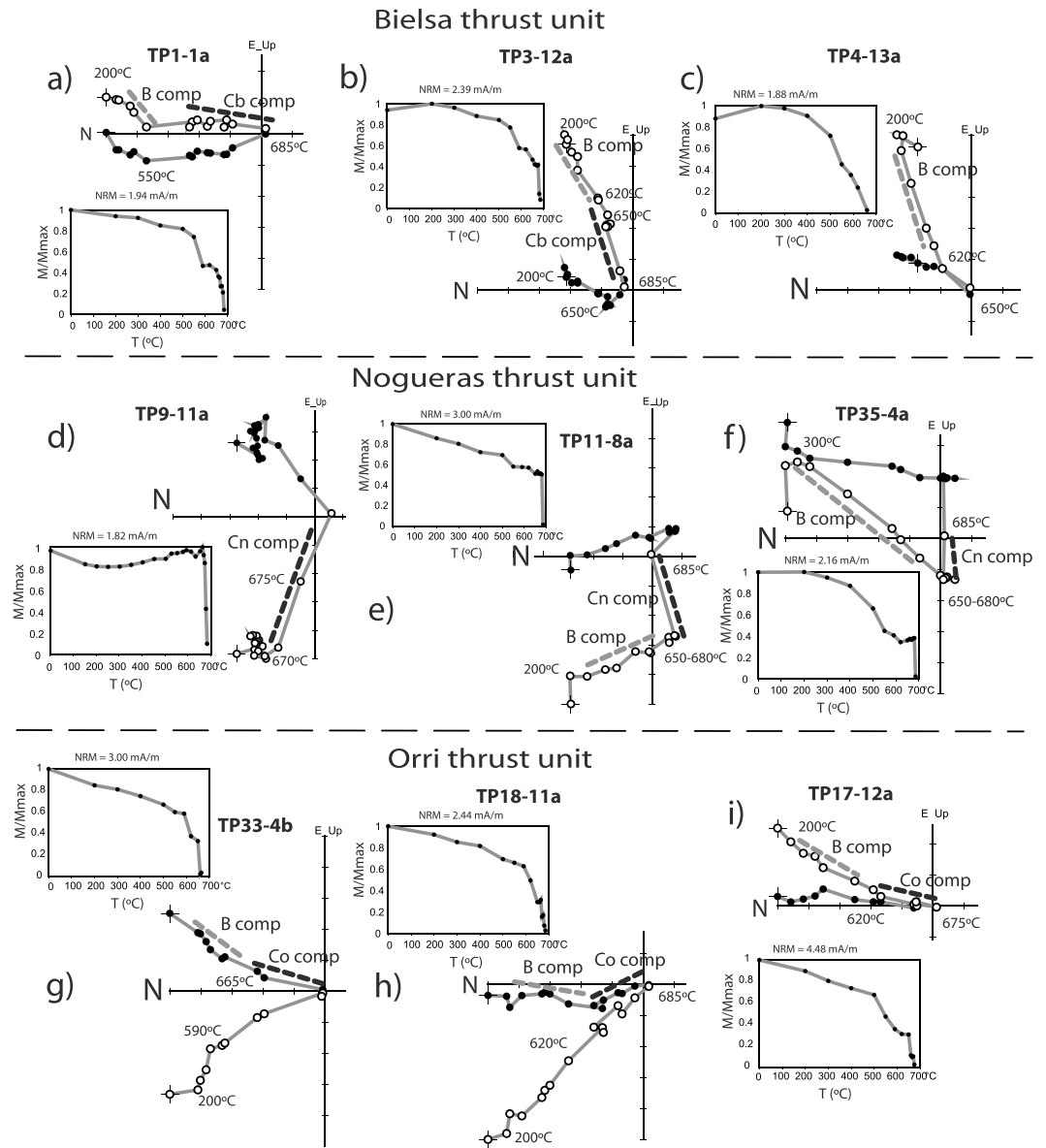


Figure 5. Paleomagnetic results from the stepwise thermal demagnetization in orthogonal plots. Diagrams from the different sampled thrust sheets are presented (geographic coordinates). The magnetic intensity decay during stepwise demagnetization is also shown. In the orthogonal diagrams, black (white) circles are projected on the horizontal (vertical) plane. B and C components are highlighted in gray and black, respectively. Note that only component C was distinguished in the sample in Figure 5d.

component B is still largely scattered. A more detailed analysis of the paleomagnetic data in each sampled thrust unit is described in the following sections.

4.2.1. Bielsa-Bono Thrust Sheet

Component C (named Cb in the Bielsa-Bono thrust sheet) was well isolated in only two out of four sites in this thrust sheet. To better constrain the average orientation of this component, we considered data from seven previous (Oliva-Urcia et al., 2012), sampling sites located to the west of our study area (in Lower-Middle Triassic red beds of the Bielsa-Bono thrust, see location in Figure 2d). Component Cb displays a large dispersion in geographic coordinates and a better grouping after tectonic correction: it trends N-S, plunges shallowly to the north (Dec = 355°, Inc = 09°, $\alpha_{95} = 11^\circ$, $k = 21$, $N = 9$, Figure 6b), and shows normal and reverse polarities.

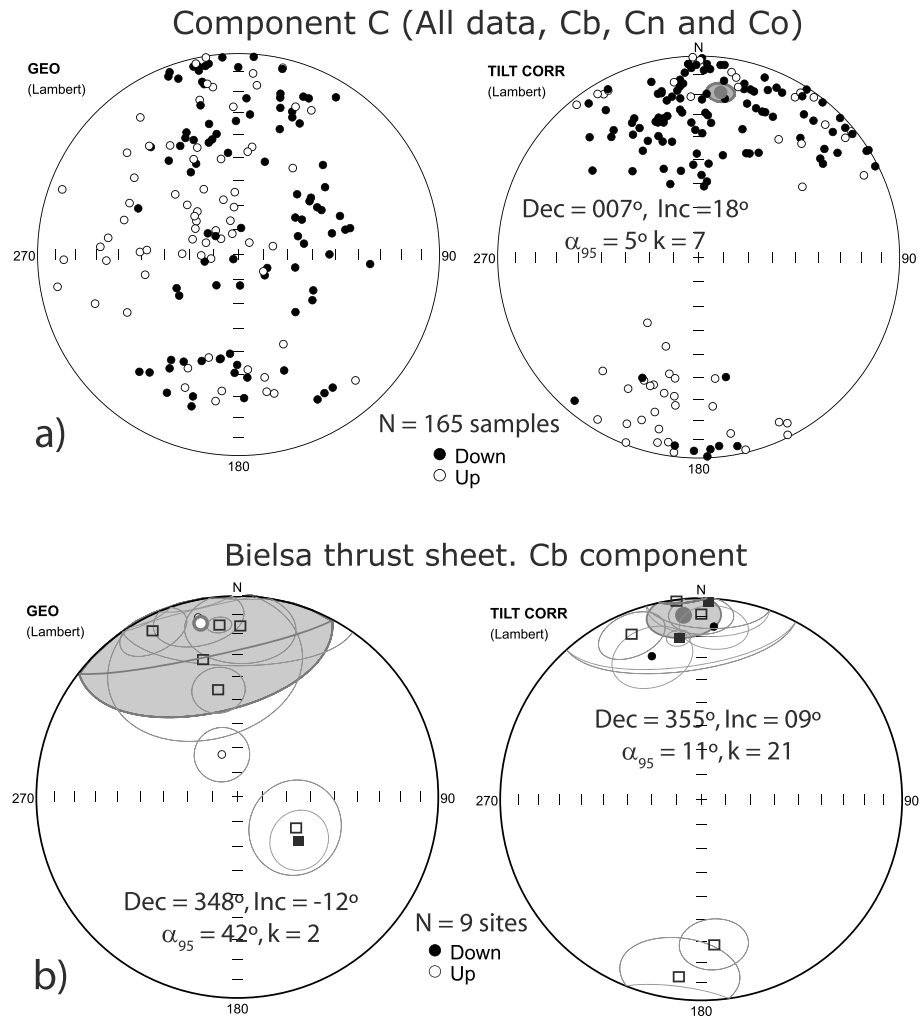


Figure 6. (a) Summary of paleomagnetic vectors calculated for component C for the whole sampling set (a, sample scale) and for the Bielsa-Bono thrust sheet (b, site scale). The equal-area plots on the left show the directions of the components before tectonic correction, whereas the equal-area plots on the right show the orientation after tectonic correction. The mean values were calculated after normalizing reverse polarity samples. In Figure 6b, two of the sites are from this study, and seven (square symbols) are from Oliva-Urcia et al. (2012).

Component B was defined in three sampling sites and shows a wide dispersion in either geographic coordinates or after bedding correction.

4.2.2. Nogueras Thrust Sheet

The C component (Cn in the Nogueras thrust sheet) was defined in 12 (out of 16) sampling sites, distributed throughout the four minor-scale thrust slices forming the Nogueras Zone (see Figure 3a). In geographic coordinates, this component displays a strong dispersion but shows a better grouping after bedding correction: it is NNE trending and subhorizontal to slightly dipping (Dec = 023°, Inc = 9°, $\alpha_{95} = 12.5^\circ$, $k = 13$, $N = 12$, Figure 7a), with some dispersion both in declination and inclination. It shows normal and reverse polarities in 6 and 3 sites, respectively, whereas dual polarities have been defined in the 3 remaining. The average normal (Dec = 027°, Inc = 5°, $\alpha_{95} = 7^\circ$, $k = 9$) and reverse (Dec = 192°, Inc = -19°, $\alpha_{95} = 7.5^\circ$, $k = 12$) polarity vectors are approximately antipodal (Figure 7c) but do not pass the McFadden and McElhinny (1990) reversal test. This is due to the directional variability that this component shows after tectonic correction and that probably results from (i) the inclination shallowing effect (Garcés et al., 1996; Tan & Kodama, 2002, among others) and (ii) a declination scatter due to actual or apparent differential VARs (Pueyo, Oliva-Urcia, et al., 2016, and references therein).

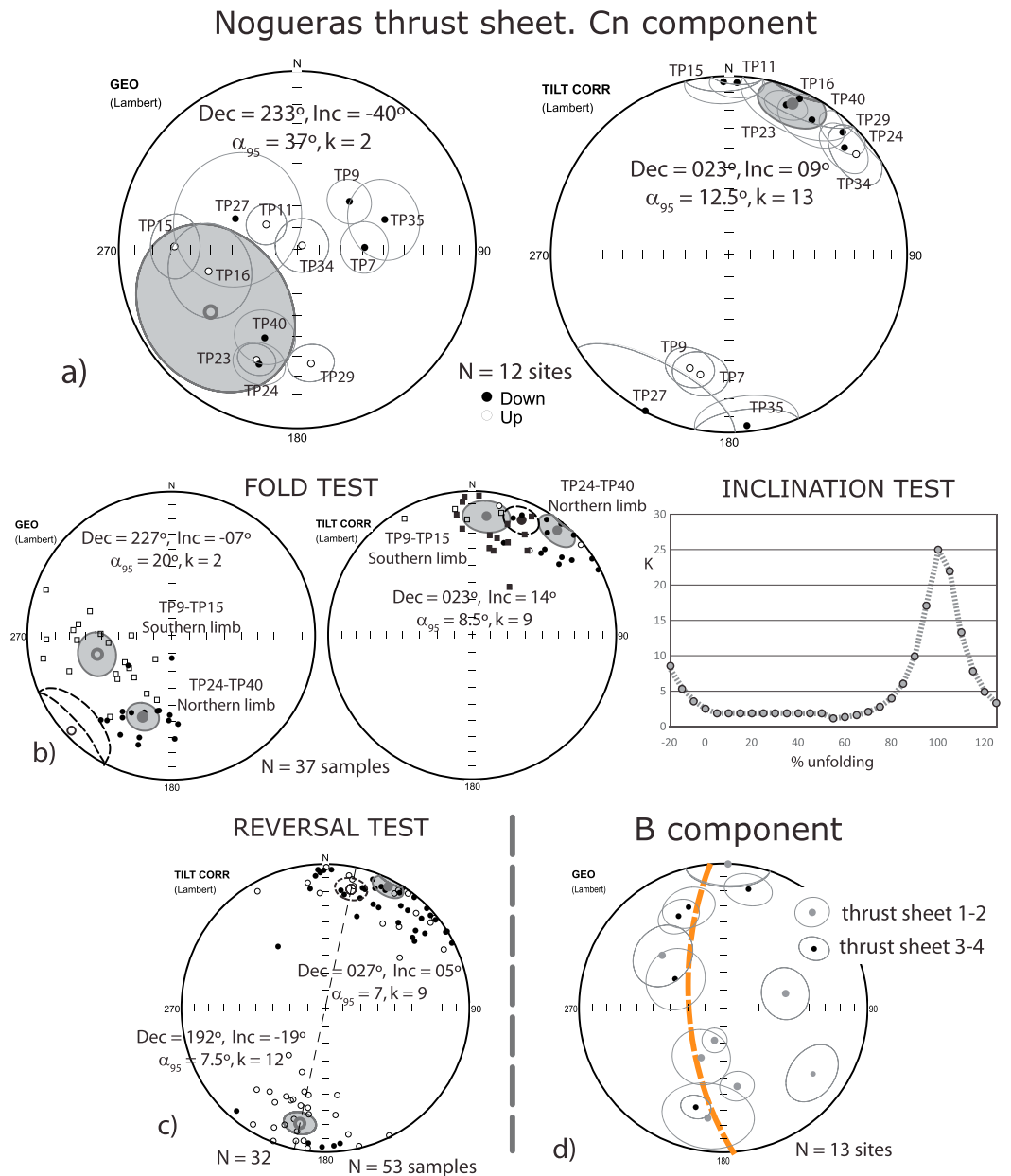


Figure 7. (a) Summary of results for component C in the Nogueras thrust sheet (Cn). Site mean directions before (left) and after (right) tectonic correction. (b) Fold and inclination tests (sample scale) for component C in the Nogueras thrust sheet (kilometric-scale synformal anticline in thrust sheet 2, see Figures 3a and 3c). The black dashed symbols represent the average component for both limbs before and after tectonic correction. (c) Reversal test for component C in the Nogueras Zone. (d) Mean site directions of component B in geographic coordinates.

Fold and inclination tests were carried out for the hanging wall synformal anticline cropping out in thrust sheet 2 (Figure 7b, see location of the thrust sheet in Figures 3a and 3c; statistics are shown in Table 3, fold test 1). The fold test is positive at the 99% level of confidence (Table 3), and the inclination test shows the best grouping after 95% of unfolding, thus indicating that the magnetization was acquired before folding. The conglomerate test performed in site TP28 displays nonsignificant, random results for both paleomagnetic components in the clasts and the matrix, probably because of their low paleomagnetic quality and coarse grain size of the matrix.

The B component shows a wide dispersion in geographic coordinates and is approximately distributed along a N-S striking girdle that dips steeply to the west, perpendicular to the regional fold axis (Figure 7d). The

Table 3
Fold Test (FT) Results

Sector	Sites	Comp.	N	In situ			After bedding correction					Fold test statistics		
				D	I	α_{95}	k	D	I	α_{95}	k	f	F	Fold test result
FT 1	N limb	Cn	17	199	40	9	19	39	7.5	9	17	BTC: 2.4609	95% = 0.0894	Positive 99%: prefolding
	S limb		20	254	-47	11	9	8	19	11	10	ATC: 0.1235	99% = 0.1406	
	N + S limbs		37	227	-7	20	2	23	14	8.5	9			
FT 2	N limb	Co	4	356	22	22.5	18	352	33	13	51	ATC: 0.1110	95% = 0.6475	Positive 95%: prefolding
	S limb		3	355	-21	32	16	355	25	29	19	BTC: 1.5001		
	N + S limbs		7	356	4	23	8	354	29	11	33			
FT 3	N limb	Co	10	348	6	4.5	117	343	30	4.5	117	ATC: 0.0966	95% = 0.1927	Positive 95%: prefolding
	S limb		9	243	40	7	56	349	25	9	34	BTC: 3.6893		
	N + S limbs		19	346	22	8	17	346	28	5	53			
FT 4	N limb	B	6	3	25	14	23	357	51	14	23	ATC: 0.2282	95% = 0.3949	Positive 95%: prefolding
	S limb		5	359	56	13.5	33	5.5	38	15	28	BTC: 1.1565		Solution with more statistical confidence = 70% unfolding
	N + S limbs		11	2	39	13	13	1.5	45	10	23			

Note. FT1 to FT4 refer to the structure where the fold test is applied (see comments in the text). For each structure, Northern (N) and southern (S) fold limbs are considered separately and together (N + S); sites considered for the test, name of the paleomagnetic component (Comp.), N refers to the number of samples (FT1, FT2, and FT3) or sites (FT4) considered in the fold test. Declination (D), Inclination (I), and the corresponding fisherian parameters (α_{95} and k) for the average, in situ and after bedding correction. f: McFadden and Jones (1981) fold test statistical parameter; F: 95 and 99% significance level value of f. The last column is the fold test results.

clustering of data does not improve after bedding correction, suggesting a syn-folding acquisition (and therefore a Cenozoic age) for this component. Considering the Cenozoic reference direction (see section 4.3) and the tilting path of bedding during folding, we defined the polarity of the B component: it is reverse in thrust sheets 1 and 2 (except in sites TP15 and TP9, toward the western termination of the thrust unit) but normal in thrust sheets 3 and 4 (Figure 3a).

4.2.3. Orri Thrust Sheet

The Co component (C component in the Orri thrust unit) displays, as in the previous thrust sheets, a better grouping after bedding correction (Dec = 347°, Inc = 25°, α_{95} = 13°, k = 17, N = 9) than in geographic coordinates (Dec = 349°, Inc = 4°, α_{95} = 25°, k = 5, N = 9) (Figure 8a). In one site, normal and reverse polarities have been observed (TP17; Table 2). Disregarding this site, and after bedding correction, a dominant normal polarity is recognized for the whole thrust sheet. The conglomerate test for site TP10 indicates that the magnetization carried by the clasts has a random distribution (α_{95} = 132°; k = 1.33), whereas that of the matrix shows a well-grouped direction (α_{95} = 16°; k = 25), suggesting a primary origin for the magnetization (Figure 8b).

The B component was isolated in nine sites and shows a considerable dispersion either in geographic (Dec = 010°, Inc = 13°, α_{95} = 31.4°, k = 3.2, N = 9; Figure 9a) or tectonic coordinates (Dec = 010°, Inc = 33°, α_{95} = 28, k = 3.9, N = 9).

Fold tests were carried out in this structural unit considering (i) a hectometric-scale syncline in the northern part of the Orri unit (sites TP18 and TP19, Figure 8d and Table 3, fold test 3, for component C; Figure 9b and Table 3, fold test 4, for component B) and (ii) the hanging wall anticline related to the Orri thrust (Figures 3c and 8c and Table 3, fold test 2, for component C). Both fold tests are positive for component C indicating that it was acquired prior to folding and thrusting. Conversely, the B component has a syn-folding character, with the best grouping at about 70% of unfolding (Table 3 and Figure 9b).

4.2.4. Summary of Results

Considering the observations previously explained (positive fold and conglomerate tests and pseudoantipodal normal and reverse mean directions), a primary origin and an Early Triassic age are inferred for component C. Slight but statistically significant differences in the average orientation of this component are observed in the different thrust sheets: Dec = 355°, Inc = 9°, α_{95} = 11°, k = 21 (N = 9) in the Bielsa-Bono unit; Dec = 023°, Inc = 9°, α_{95} = 12.5°, k = 13 (N = 12), in the Noguerras Zone; and Dec = 347°, Inc = 25°, α_{95} = 13, k = 17 (N = 9) in the Orri thrust sheet.

Previous data from the Noguerras unit (Bates, 1989) can be here reevaluated. The individual site means of the high-temperature (H) component from this study were very poor and scattered, partially due to the small number of analyzed samples (5 on average). After filtering previous data from the Noguerras unit (Bates, 1989) and considering only sites with $\alpha_{95} < 20^\circ$, an average orientation Dec = 027.9, Inc = 16.8 (α_{95} = 15.8°, k = 11.6, N = 8) is obtained after tectonic correction; this direction is in well agreement with our data in the Noguerras unit.

Component B shows a wide dispersion at regional scale, both in geographic coordinates and after bedding correction. Its distribution in the Noguerras unit and the fold test results in the Orri thrust sheet suggest that component B

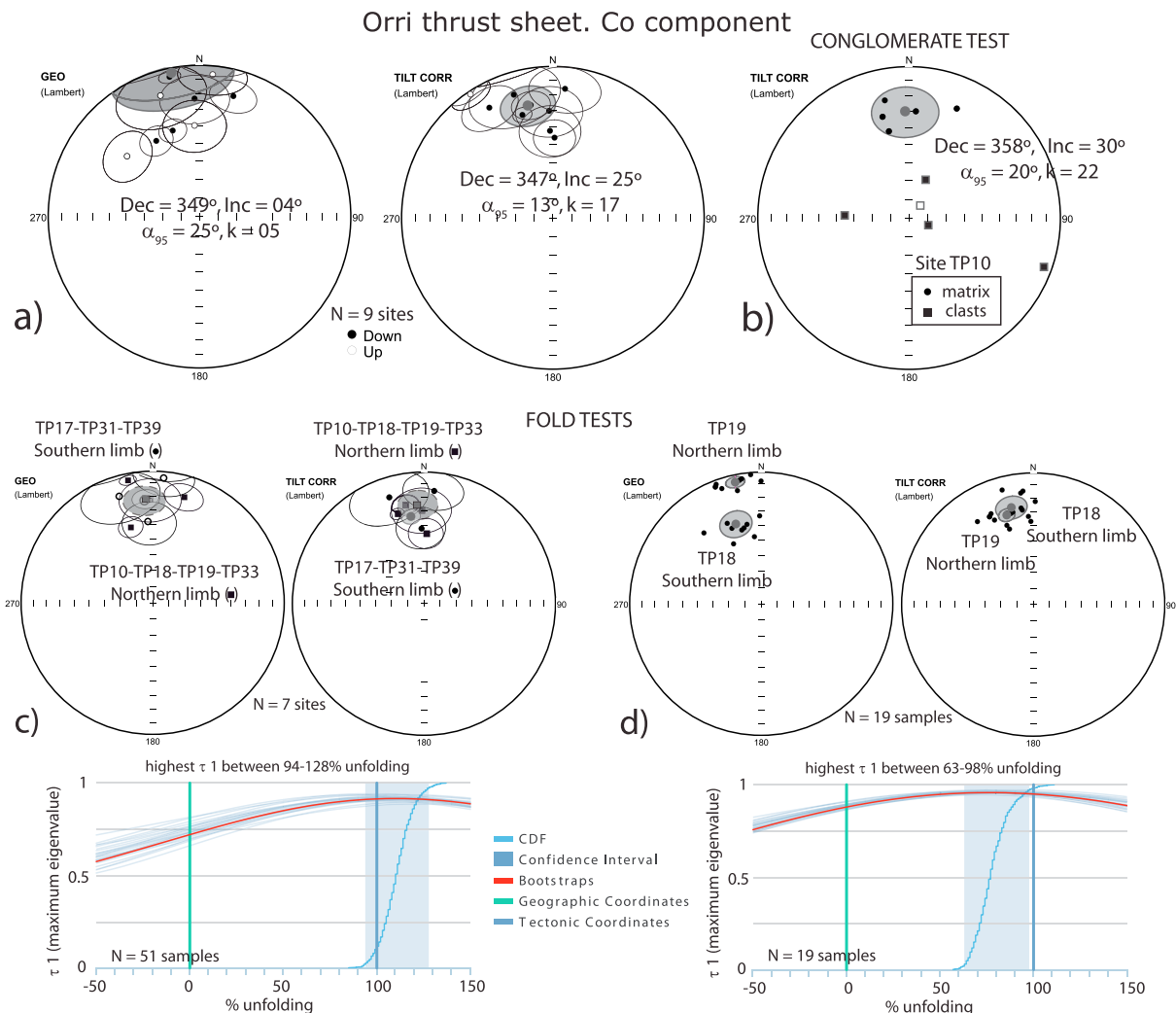


Figure 8. Summary of results for component C (Co) in the Orri thrust sheet. (a) Site mean directions before (left) and after (right) tectonic correction. (b) Positive conglomerate test for component Co. (c) Graphical and stepwise fold tests for component Co in the hanging wall anticline of the Orri thrust. Note that component C in the southern limb is upwards plunging (upper hemisphere) in geographic coordinates. The stepwise fold test was carried out at the sample scale, whereas the McFadden and Jones (1981) fold test (Table 3) was carried out at the site scale to avoid underrepresentativeness of sites TP10 and TP17, with a lower number of samples. Both fold tests are positive. (d) Graphical and stepwise fold tests (sample scale) for component Co in the syncline sampled in sites TP18 and TP19. Statistics for fold tests are included in Table 3. Bootstrapped, stepwise fold tests were carried out using the online platform Paleomagnetism.org (Koymans et al., 2016).

corresponds to a diachronous, syn-orogenic remagnetization acquired contemporary to folding and thrusting during Eocene-Oligocene times (see analysis of the timing and origin of this remagnetization in the supporting information; Henry et al., 2004; Pueyo-Anchuela et al., 2013; Pueyo et al., 2016; Pullaiah et al., 1975; Ramón et al., 2016; Shipunov, 1997).

4.3. Paleomagnetic References

To quantify the amount of VARs, the Early Triassic and Eocene-Oligocene reference directions were calculated for a common reference point centered in the study area at 42°28'15"N and 0°35'52"E (Las Paules village). The Early Triassic reference is 345°/14° ($N = 5, \alpha_{95} = 5.8^\circ, k = 138.3$), calculated from paleopole data by Parés et al. (1996), Schott and Perés (1987), and Osete et al. (1997, compiled in Osete & Palencia-Ortas, 2006). The Eocene-Oligocene reference, chosen in accordance to known alpine deformation ages in the region, is 000°/47° ($N = 7, \alpha_{95} = 7^\circ, k = 66$), calculated from data in Taberner et al. (1999) and from normal average components in four different magnetostratigraphic profiles (Maians-Rubió, Costa et al., 2010; Miralles-La Tossa, Costa et al., 2012; Montserrat, Gómez-Paccard et al., 2012; and Moia-Santpedor, Costa et al., 2011), all located in the northeastern part of the south Pyrenean Ebro foreland basin.

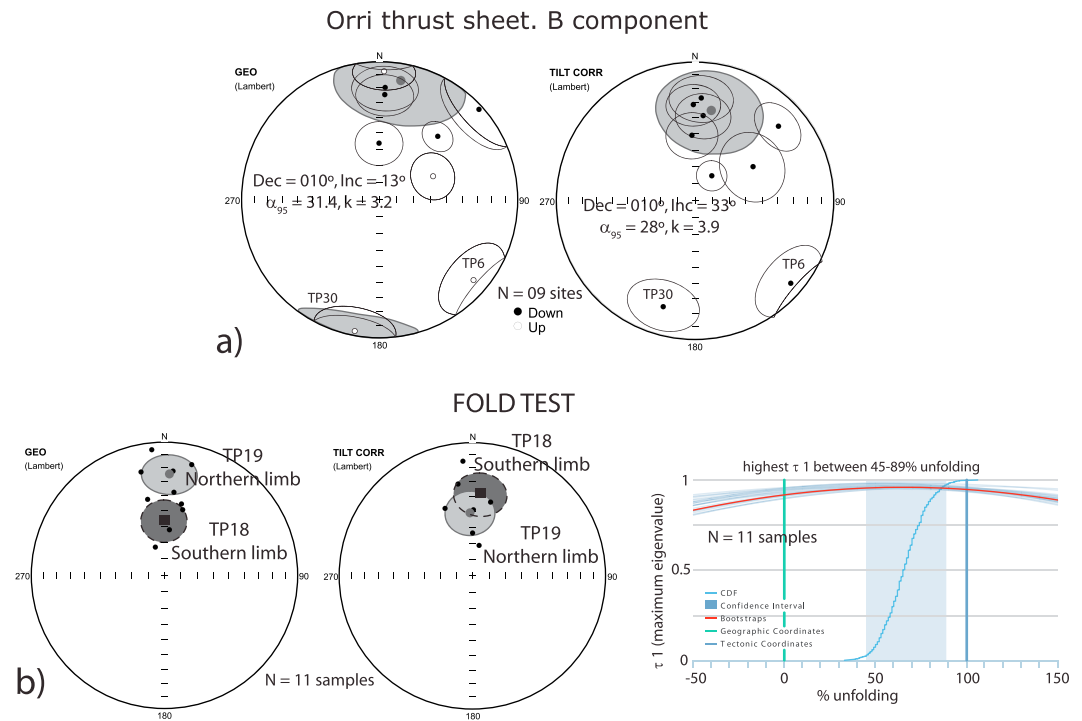


Figure 9. Summary of results for component B in the Orri thrust sheet. (a) Site mean directions before (left) and after (right) tectonic correction (after transposing sites TP6 and TP30). (b) Graphical and stepwise fold tests (sample scale) for component B in the syncline sampled in sites TP18 and TP19. Statistics for fold tests are included in Table 3. CDF = cumulative distribution function.

5. Discussion

5.1. Magnitude of VARs

VARs across the study area are calculated from the comparison between the Early Triassic reference direction and the primary C component. As previously described, component B occurs throughout the whole studied domain, but its syn-tectonic character prevents its direct interpretation in terms of finite VARs.

The negative reversal test (McFadden & McElhinny, 1990) for component C in the Nogueras unit reveals that its directional record is likely influenced by the inclination shallowing effect (Garcés et al., 1996; Tan & Kodama, 2002, among others) that can produce a considerable deflection in the measured inclinations but negligible deviation in the declination (i.e., precluding the accurate calculation of horizontal but not of VARs). When compared to the reference direction, primary inclinations in the study area are shallower or equal to the expected Triassic inclination (79% of values are bracketed between 15 and 0°). Higher values can be considered as anomalous and could result from the deformation of the magnetic remanence during shortening (Borradaile, 1992). Sites showing these anomalously high inclinations (>40°) are discarded for the calculation of VARs in this study (TP33 and TP31, see Table 2), whereas sites displaying inclinations ranging between 30 and 40° (TP9, TP7, TP10, and TP19) are considered with care.

5.1.1. Thrust-Sheet Average Rotations

The mean orientation of component C in the Bielsa-Bono, Orri, and Nogueras units has been considered (Figure 10a) to roughly evaluate the regional-scale VARs in the different thrust sheets. The mean of the C component shows a clockwise rotation of +10° ($\pm 17^\circ$) in the Bielsa-Bono thrust sheet (D/I of 355°/09°; $\alpha_{95} = 11$; $k = 21$) and +38° ($\pm 19^\circ$) in the Nogueras Zone (D/I of 023°/09°; $\alpha_{95} = 12.5$; $k = 13$). The reported errors in the rotation values are calculated as the addition of the uncertainty in declination of the average paleomagnetic vector ($\Delta D_{obs} = \alpha_{95}/\cos I$) and the reference ($\Delta D_{ref} = 5/\cos 14$).

The clockwise rotation in the Nogueras Zone is statistically significant and consistent with the rotations obtained in previous paleomagnetic studies, both in the Lower-Middle Triassic units of the Eastern Nogueras

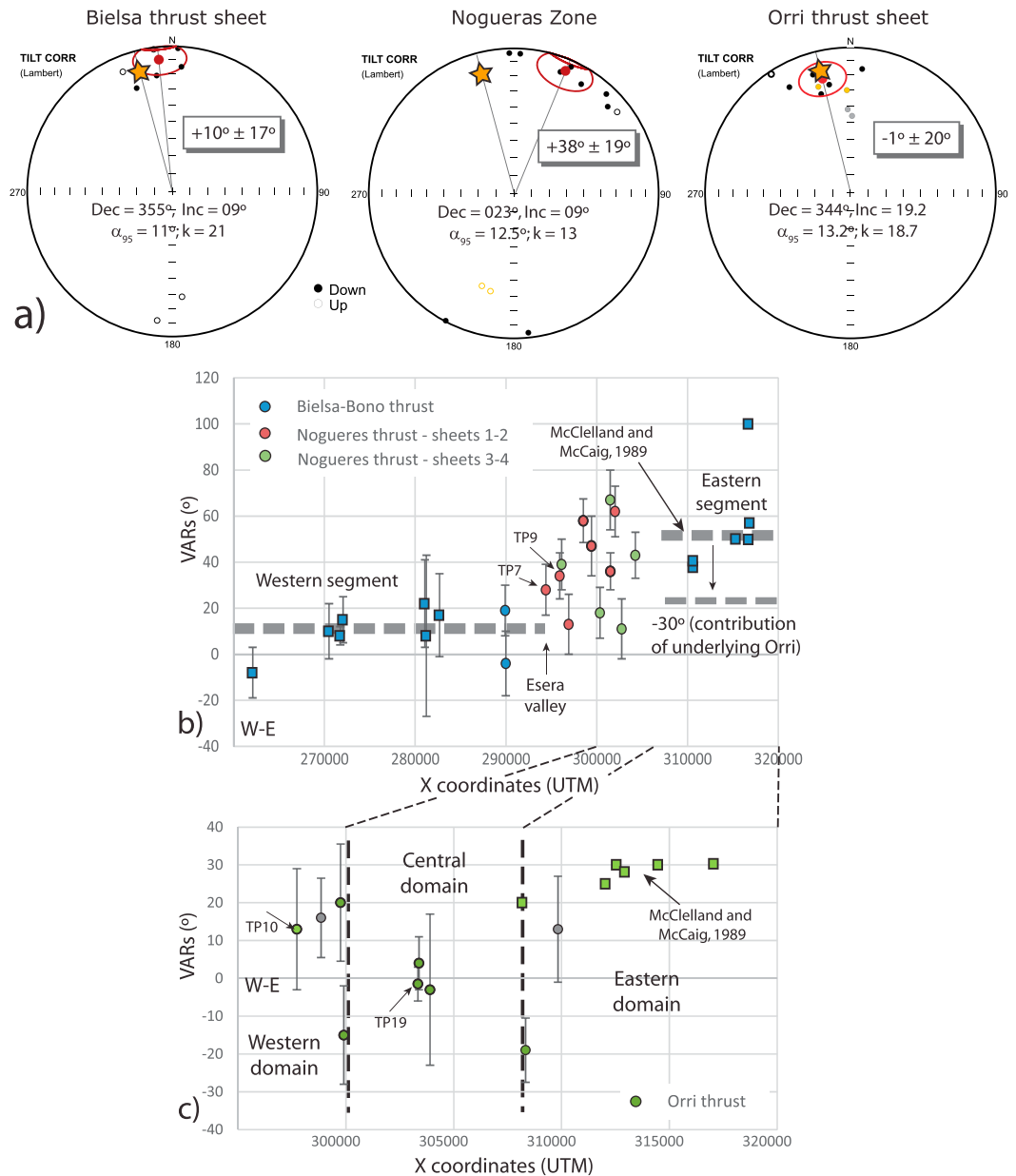


Figure 10. (a) Average of the site mean directions for the C component in each sampled thrust sheet and comparison to the Early Triassic reference (orange star). Sites with inclinations higher than 40° were disregarded to calculate the average (shown in light gray). Average values in the figure take into account sites where inclination after tectonic correction ranges between 30° and 40° (in yellow). When these sites are ruled out, a mean Dec = 024, Inc = 04 ($N = 10$, $\alpha_{95} = 13.4$, $k = 12.6$) is obtained for the Nogueras Zone, whereas the Orri thrust sheet displays an average Dec = 342, Inc = 14.7 ($N = 5$, $\alpha_{95} = 17.4$, $k = 16.2$). Declinations differ 1 and 2° , respectively, from the mean values shown in Figure 10a. (b and c) X coordinates (longitude, UTM, 31 N zone) versus rotation values in the Bielsa-Bono thrust and the Nogueras unit (b) and the Orri thrust (c). Error bars are α_{95} angles in the represented sites. Gray dots refer to sites with inclinations higher than 40° , whereas sites where inclination after tectonic correction ranges between 30° and 40° are labeled (TP7, TP9, TP10, and TP19). Sites from this study are represented by dots, whereas squares represent sites from previous studies.

Zone ($+45^\circ$, Bates, 1989) and in the Stephanian-Permian volcanic units ($+37^\circ$) underlying the Triassic red beds (thrust sheet 3 in Figure 3a; Izquierdo-Llavall et al., 2014). The Orri unit shows a mean for the C component that overlaps the Early Triassic reference, indicating the absence of a regional, average VAR in the portion of the thrust sheet sampled in this study ($-1 \pm 20^\circ$). These average rotation values at the thrust sheet scale indicate an increase of rotations from the base to the top of the thrust stack, with the Nogueras and Bielsa-Bono

units being strongly and slightly rotated, respectively, and the Orri unit being unrotated. This distribution of VARs is in agreement with the piggyback thrust sequence in the central Axial Zone (Muñoz, 1992).

5.1.2. Lateral Variation of Rotation Values. Implications for the Development of the Basement Antiformal Stack in the Axial Zone

To evaluate how VARs vary along strike in the studied thrust units, we took into account the new data presented in this study plus previous paleomagnetic data in the Orri thrust sheet (McClelland & McCaig, 1989a, 1989b) and the Bielsa-Bono unit (Oliva-Urcia et al., 2012) and its lateral continuation (Bono thrust, McClelland & McCaig, 1989a, 1989b, see location in Figure 2d). Considering the whole data set, we determined that VARs in the Bielsa-Bono thrust unit (Figure 10b) change along strike, with a general increase from west to east that can be described through a western thrust segment characterized by an average clockwise rotation of $\sim 10^\circ$ and an eastern thrust segment displaying a strong clockwise rotation ($\sim 50^\circ$, Figure 10b).

Rotations and differential shortening are commonly related (Allerton, 1998; McCaig & McClelland, 1992). When the considered sections are parallel to the transport direction, then a simplified estimation can be done with the following equation (Pueyo et al., 2004):

$$\Delta S = S_{c2} - S_{c1} = 2D \cdot \sin(\beta/2)$$

where S_{c1} and S_{c2} are the shortening values along two different cross sections, D is the distance between them (along the footwall cutoff), and β is the rotation value (see Figures 10b and 10c). If two sections at a distance of 10 km from each other are considered across the western segment of the Bielsa-Bono thrust (average rotation of $\sim 10^\circ$), a small shortening difference of 1.7 km between them can be calculated. Conversely, if two sections separated 10 km are considered across the eastern thrust segment (average rotation of $\sim 50^\circ$), the estimated shortening difference would be 5 times higher (8.5 km).

Regarding the Nogueras unit, Average thrust-slice rotations suggest a progressive increase from the base to the top of the thrust system (i.e., the upper thrust units showing stronger VARs), although this general trend fails in thrust sheet 3 (see location in Figure 3a) that is less rotated than the overlying and underlying units. This general rotation pattern is in agreement with a piggyback thrust sequence that should be understood in a scenario of small, varying wavelength thrust sheets ending up/relaying laterally and therefore leading to along-strike rotation changes. On the contrary, wider thrust sheets such as the western segment of the Bielsa unit display more constant rotation values through longer thrust portions (Figure 10b). VARs in the Nogueras unit have been represented in Figure 10b, and (despite their variability) they lie in the general trend previously defined for rotations in the Bielsa-Bono thrust. This observation supports the idea of the Bielsa-Bono thrust being the root of the lower Nogueras units along the study area. In turn, the stronger, clockwise VARs recorded to the East of the Ésera Valley (Figure 10b) evidence that the eastward increase in the displacement of the upper thrust units in the Axial Zone is one of the key factors controlling the occurrence of downward facing structures in the Nogueras Zone and the along-strike geometrical change in the basement thrust system (Figure 1a).

Furthermore, as previously introduced, the occurrence of the Orri thrust in the eastern part of the study area also contributes to the vertical stacking of thrust units and the development of the Axial Zone antiformal stack (Figure 1b). The Orri thrust emerges along the Ésera valley and, from the rotational point of view, it can be roughly divided into three along-strike domains (Figure 10c): a western and eastern domains characterized by slight to moderate clockwise VARs (10 to 20° in the west and 20 to 30° in the east) and a central, unrotated, or slightly counterclockwise rotated zone. Clockwise VARs in the western domain are consistent with the termination of the Orri unit along an oblique ramp, as inferred from structural data and geological mapping (Izquierdo-Llavall, Casas-Sainz, et al., 2013). The eastern domain (defined from data by McClelland & McCaig, 1989a, 1989b) is located to the east of the eastern termination of the Nogueras unit in the study area, meaning that rotations in the former domain are not contributing to rotations in the latter one. Conversely, the strong clockwise rotation in the hanging wall of the Bono thrust (eastern segment, Figure 10b) is likely the sum of the Bono thrust-sheet rotation plus the rotation of the underlying Orri unit (eastern domain, Figure 10c).

From the along-strike analysis of rotations in the studied thrust system, and considering the end-members shown in Figure 1, we suggest that the lateral transition in the Axial Zone from an imbricate thrust system to an antiformal stack results from an intermediate scenario. It is promoted by both (i) the eastward

increase in thrust displacement along the upper thrust units (the Bielsa-Bono thrust, understood as the root zone for the lower Nogueras unit) and (ii) the emergence of new thrusts (i.e., the Orri thrust) that enhance vertical stacking to the east. Increasing thrust displacements to the east are consistent with the overall structure of the western-central Pyrenees, with related shortening values that are higher in the central part (148 km, Muñoz, 1992; 165 km, Beaumont et al., 2000) but decrease across the central-western (100 km, Martínez-Peña & Casas-Sainz, 2003) and western Axial Zone (80 km, Teixell, 1996; 115 km in the hyperextended scenario, Teixell et al., 2016).

5.2. Basement-Cover Relationships: Implications for the Rotations of the SPCU

The basement rotation values here presented allow us to hypothesize about the origin of the strong, clockwise rotations in the Mesozoic-Cenozoic units of the western SPCU. This domain is located to the south of the study area (Figure 2) and above the regional detachment level represented by the Keuper units. Rotation values in these thrusts reach maximum values of 50 to locally 70° (the latter in the Mediano anticline, Muñoz et al., 2013). They are nearly coincident throughout the Bóixols, Montsec, and Sierras Marginales units, consistently with a late rotation due to differential thrust displacement in the southernmost thrust unit (Garcés et al., 2016): the Bóixols and Montsec units were originally nonrotational (i.e., they did not rotate during their emplacement) but were, latter, passively rotated and transported in the hanging wall of the Sierras Marginales structure (Garcés et al., 2016; Muñoz et al., 2013). The rotated domain has a triangular shape in map view (Figure 11) and it is characterized by a rough rotation increase from west to east (Garcés et al., 2016; Muñoz et al., 2013) as also observed in the basement units to the north (Figures 10b and 10c). Rotations in the western SPCU mostly occurred during Eocene times (Mochales et al., 2012; Muñoz et al., 2013), whereas a minor (~10°), late rotation event took place during Priabonian-Oligocene (Muñoz et al., 2013).

Assuming that basement rotations accumulated in the southern part of the Axial Zone (10° to 50°, see Figures 10b and 10c) were fully transferred to cover units (see discussion below), an additional cover rotation ranging from 20° to 40° is required to explain paleomagnetic results at the western SPCU. The basement thrusts accommodating the differential displacement necessary to produce this additional rotation in the cover should be located to the north of the sampled domain (i.e., the Gavarnie thrust or the northern basement thrusts indicated in Figures 2b and 2c) and therefore be earlier than the Bielsa-Bono-lower Nogueras and Orri thrusts (Figure 2d). Among them, the Gavarnie basement thrust has been documented to register maximum clockwise rotations of +26° to the west of the study area and an average or regional-scale background rotation of +15° (Izquierdo-Llavall et al., 2015; Oliva-Urcia & Pueyo, 2007; Pueyo, 2000).

Taking all of this into account, and considering thrust activity ages given in previous studies (Beamud et al., 2011; Mellere & Marzo, 1992; Muñoz, 1992; Séguret, 1972; Verges & Muñoz, 1990), the following four stage evolution for the central Axial Zone and the western SPCU can be proposed (schematically depicted in Figure 11): (1) nonrotational emplacement of the northern basement thrusts (Figure 2) that transfer shortening to the Bóixols (Late Cretaceous) and Montsec (Paleocene-late Ypresian) cover thrust units; (2) rotational emplacement of the Gavarnie basement thrust during early Eocene, coevally to the Triassic-detached Sierras Marginales structure and an early, weak (~ + 15°) rotation in the southern Pyrenees; (3) rotational emplacement of the Bielsa-Bono-lower Nogueras thrust units (~ + 10° to +40°, in average Figure 10b) producing variable VARs across the western SPCU (late Eocene); and finally, (4) formation of the Orri thrust (late Eocene-Oligocene) accounting for the differential displacement required to fulfill rotations in the cover units of the SPCU (maximum rotation of +30°, see Figure 10c).

The extent and distribution of rotations related to basement thrusting differ depending on the considered thrust sheet. Paleomagnetic data suggest rotations are widespread and almost constant along the strike of the Gavarnie thrust (Figure 11b) that produced an approximately homogeneous rotation of both overlying basement thrusts (+15 and 26° in the Mesozoic cover of the northern axial Zone, Aure sector in Oliva-Urcia et al., 2012) and overlying Meso-Cenozoic units to the South (Izquierdo-Llavall et al., 2015; Oliva-Urcia & Pueyo, 2007; Pueyo, 2000). Conversely, the lower Nogueras thrust units, formed by minor-scale thrusts that relay along strike, produced rotations that are variable at the thrust sheet scale and affect more local domains (i.e., the rotated domains have a limited lateral extent, Figure 11c). An intermediate scenario is represented by

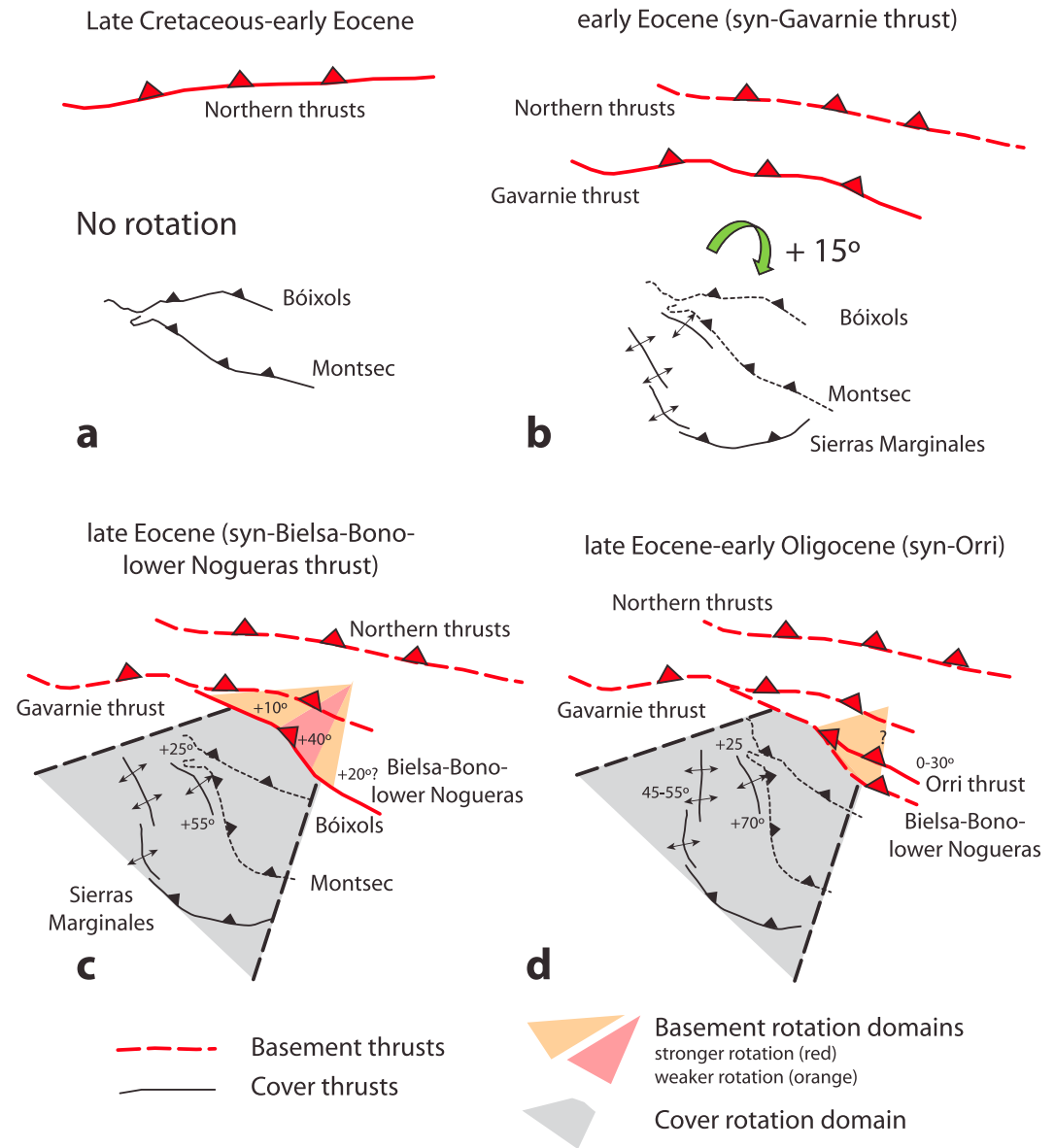


Figure 11. Schematic evolution of basement and cover thrusting in the western SCPU and the central Axial Zone. Solid lines indicate active thrusting; dashed lines indicate inactive thrusts.

the Bielsa-Bono and the Orri thrusts, related to variable rotations that can be roughly constant along kilometric-scale thrust segments (Figures 10b and 10c).

How rotations are transferred from basement to cover units could be understood through two different mechanisms: (i) a passive, coupled rotation of cover units on top of basement units or (ii) a decoupled transfer of differential basement thrust displacements that is resolved in the overlying units through differential displacements in cover, thin-skinned thrusts. The first mechanism requires that the décollement separating cover and basement units remained inactive and allowed to fully transfer rotations from the basement to the cover (i.e., rotation values in cover and basement units being equal). Several plausible reasons can be invoked for that mechanism, such as the décollement being too thin in comparison to the overlying cover units (Pla et al., 2017) or the deformation velocity being too fast to permit its fully ductile behavior (Couzens-Schultz et al., 2003). Besides, the early compartmentalization of the décollement during precontractional stages (due to basement faulting or early evaporite flow; López-Mir et al., 2014; McClay et al., 2004) is an additional factor that can considerably diminish décollement effectiveness. The second mechanism can

produce differential rotations between the basement and the cover depending on how the differential shortening transferred from the basement is accommodated in the cover units. If both basement and cover thrusts are forward verging, the differential shortening should produce similar rotations above and beneath the décollement. On the contrary, if shortening in cover units is partly resolved through backthrusting, VARs in the cover will be smaller than those in the basement. Considering that the sum of basement rotations in the central Axial Zone roughly equals VARs in cover units, we can hypothesize that in a scenario of decoupled rotation transfer, passive backthrusting was not a major process across the western SPCU.

6. Conclusions

The paleomagnetic data presented in this study allow for the characterization of thrust kinematics in the structural transition between the western-central and the central Axial Zone. This transition is defined by a basement system that laterally changes from an imbricate thrust system to the West to an antiformal stack displaying frontal, downward facing structures to the East (the Nogueras Zone).

Two stable magnetization components were defined in the Lower-Middle Triassic red beds unconformably overlying the Paleozoic basement of the studied area: (1) a secondary, intermediate-temperature component that is syn-orogenic and (2) a primary component that unblocks at slightly higher temperatures. Both paleomagnetic components are found across the three considered thrust units (the Nogueras Zone, the Bielsa-Bono thrust and the underlying Orri unit). The primary component displays two polarities at regional and site scale and shows thrust-scale, mean rotations ranging from 0 to +38°, the higher values defined across the Nogueras Zone. Mean VARs increase from the base to the top of the thrust system, accordingly to a piggy-back sequence. Rotation estimates in this study are integrated with previous paleomagnetic data from neighboring areas and indicate an eastwards increase in the VARs registered by the upper thrust units (Bielsa-Bono thrust and Nogueras Zone) that range from ~10° up to ~50°. This rotation values, together with structural data, suggest that the geometrical change in the Axial Zone thrust system results from the combined effect of the eastwards increment: (i) in thrust displacement along the upper thrust units and (ii) in the number of basement thrusts.

We propose a tight correlation between the VARs found in basement units and those widely documented across the cover sequence in the western SPCU. The strong rotations in the latter domain are probably the sum of an early clockwise rotation (average of 15°) related to the Gavarnie basement thrust, a subsequent rotation coeval to the emplacement of the Bielsa-Bono-lower Nogueras thrusts (reaching maximum, average values of ~+40°) and a later event related to the emplacement of the Orri unit (0 to +30°).

Acknowledgments

The authors thank Cristina García for her help during field work and Manuel Tricas for the preparation of thin sections. We also thank Josep Anton Muñoz for his clarifying explanations about the Nogueras and the Axial Zone. This study was part of the research projects CGL2009-08969, CGL2006-05817, CGL2009-10840, and CGL2012-38481 (Spanish Ministry of Education) and was included in the objectives of the predoctoral grant AP-2009 – 0554 (Esther Izquierdo, Programa de Formación de Profesorado Universitario, Spanish Ministry of Education). Funding from Instituto de Estudios Altoaragoneses is also acknowledged. B. O. U. acknowledges funding from the JAEDOC program of CSIC and ESF. Data used in section 4 are shown in Tables 1–3 from the present manuscript. The careful and constructive review by Jaume Dinarès, Graeme Taylor, and two anonymous reviewers are acknowledged and helped improving both the content and the shape of the present manuscript.

References

- Allerton, S. (1998). Geometry and kinematics of vertical-axis rotations in fold and thrust belts. *Tectonophysics*, 299(1-3), 15–30. [https://doi.org/10.1016/S0040-1951\(98\)00196-6](https://doi.org/10.1016/S0040-1951(98)00196-6)
- Barnolas, A., Gil-Peña, I., Martín-Alfageme, S., Ternet, Y., Baudin, T., & Laumonier, B. (2008). Mapa geológico de los Pirineos a escala 1:400.000. IGME-BRGM.
- Bates, M. (1989). Palaeomagnetic evidence for rotations and deformation in the Nogueras zone. Central southern Pyrenees. *Journal of the Geological Society of London*, 146(3), 459–476. <https://doi.org/10.1144/gsjgs.146.3.0459>
- Beamud, E., Muñoz, J. A., Fitzgerald, P. G., Baldwin, S. L., Garcés, M., Cabrera, L., & Metcalf, J. R. (2011). Magnetostratigraphy and detrital apatite fission track thermochronology in syntectonic conglomerates: Constraints on the exhumation of the south-central Pyrenees. *Basin Research*, 23(3), 309–331. <https://doi.org/10.1111/j.1365-2117.2010.00492.x>
- Beaumont, C., Muñoz, J. A., Hamilton, J., & Fullsack, P. (2000). Factors controlling the Alpine evolution of the central Pyrenees inferred from a comparison of observations and geodynamical models. *Journal of Geophysical Research*, 105, 8121–8145. <https://doi.org/10.1029/1999JB900390>
- Borradaile, G. J. (1992). Experimental deformation of two-component IRM in magnetite-bearing limestone: A model for the behaviour of NRM during natural deformation. *Physics of the Earth and Planetary Interiors*, 70(1–2), 64–77. [https://doi.org/10.1016/0031-9201\(92\)90161-N](https://doi.org/10.1016/0031-9201(92)90161-N)
- Caus, E., García-Senz, J., Rodés, D., & Simó, A. (1990). Stratigraphy of the Lower Cretaceous (Berriasian-Barremian) sediments in the Organyà Basin, Pyrenees, Spain. *Cretaceous Research*, 11(3), 313–320. [https://doi.org/10.1016/S0195-6671\(05\)80015-1](https://doi.org/10.1016/S0195-6671(05)80015-1)
- Chadima, M., & Hroudá, F. (2006). Remasoft 3.0 a user friendly paleomagnetic data browser and analyzer. *Travaux Géophysiques*, 27, 20–21.
- Costa, E., Garcés, M., López-Blanco, M., Beamud, E., Gómez-Paccard, M., & Larrasoña, J. C. (2010). Closing and continentalization of the south Pyrenean foreland basin (NE Spain): Magnetostratigraphical constraints. *Basin Research*, 22(6), 904–917.
- Costa, E., Garcés, M., López-Blanco, M., Serra-Kiel, J., Bernaola, G., Cabrera, L., & Beamud, E. (2012). The Bartonian-Priabonian marine record of the eastern south Pyrenean Foreland Basin (NE Spain): A new calibration of the larger foraminifers and calcareous nannofossil biozonation. *Geologica Acta*, 11(2), 177–193.

- Costa, E., Garcés, M., Sáez, A., Cabrera, L., & López-Blanco, M. (2011). The age of the "Grande Coupure" mammal turnover: New constraints from the Eocene–Oligocene record of the eastern Ebro Basin (NE Spain). *Palaeogeography, Palaeoclimatology, Palaeoecology*, *301*(1–4), 97–107. <https://doi.org/10.1016/j.palaeo.2011.01.005>
- Couzens-Schultz, B. A., Vendeville, B. C., & Wiltshcko, D. V. (2003). Duplex style and triangle zone formation: Insights from physical modeling. *Journal of Structural Geology*, *25*(10), 1623–1644. [https://doi.org/10.1016/S0191-8141\(03\)00004-X](https://doi.org/10.1016/S0191-8141(03)00004-X)
- DeCelles, P. G., Lawton, T. F., & Mitra, G. (1995). Thrust timing, growth of structural culminations, and synorogenic sedimentation in the type Sevier orogenic belt, western United States. *Geology*, *23*(8), 699–702. [https://doi.org/10.1130/0091-7613\(1995\)023<0699:TTGOSC>2.3.CO;2](https://doi.org/10.1130/0091-7613(1995)023<0699:TTGOSC>2.3.CO;2)
- Dinarès, J., McClelland, E., & Santanach, P. (1992). Contrasting rotations within thrust sheets and kinematics of thrust tectonics as derived from palaeomagnetic data: An example from the southern Pyrenees. In K. R. McClay (Ed.), *Thrust Tectonics* (pp. 235–246). London: Chapman and Hall. https://doi.org/10.1007/978-94-011-3066-0_24
- Dinarès-Turell, J. (1992). Paleomagnetisme a les unitats sudpirinenques superiors, Implicacions estructurals, PhD Thesis, Univ. of Barcelona, Spain
- Dunlop, D. J. (1972). Magnetic mineralogy of unheated and heated red sediments by coercivity spectrum analysis. *Geophysical Journal of the Royal Astronomical Society*, *27*(1), 37–55. <https://doi.org/10.1111/j.1365-246X.1972.tb02346.x>
- Fernández, O. (2004). Reconstruction of geological structures in 3D. An example from the Southern Pyrenees, PhD thesis, Univ. de Barcelona, Spain
- Fisher, R. (1953). Dispersion on a sphere. *Proceedings of the Royal Society of London, Series A*, *217*, 295–305.
- Garcés, M., García-Senz, J., Muñoz, J. A., López-Mir, B., & Beamud, E. (2016). Timing of magnetization and vertical-axis rotations of the Cotiella massif (Late Cretaceous, south central Pyrenees). *Geological Society, London, Special Publications*, *425*(1), 213–232. <https://doi.org/10.1144/SP425.11>
- Garcés, M., Parés, J. M., & Cabrera, L. (1996). Further evidence for inclination shallowing in red beds. *Geophysical Research Letters*, *23*, 2065–2068. <https://doi.org/10.1029/96GL02060>
- García Senz, J., Ramírez Merino, J. I., Navarro Juli, J. J., Rodríguez Santisteban, R., Castaño, R. M., Leyva, F., et al. (2009). Memoria explicativa de la Hoja 213 (Pont de Suert). IGME, Spain.
- García-Sansegundo, J. (1996). Hercynian structure of the axial zone of the Pyrenees through the Aran Valley cross-section (Spain-France). *Journal of Structural Geology*, *18*(11), 1315–1325. [https://doi.org/10.1016/S0191-8141\(96\)00050-8](https://doi.org/10.1016/S0191-8141(96)00050-8)
- Gisbert, J. (1983). El Pérmico de los Pirineos españoles. In C. Martínez Díaz (Ed.), *Carbonífero y Pérmico de España* (pp. 405–420). Madrid: X Congreso Internacional de Estratigrafía y Geología del Carbonífero.
- Gisbert, J., Martí, J., & Gascón, F. (1985). Guía de la excursión al Stephaniense, Pérmico y Triásico inferior del Pirineo catalán. II Congreso de Estratigrafía y Paleogeografía del Pérmico y Triásico de España, La Seu d'Urgell, 79 pp.
- Gómez-Paccard, M., López-Blanco, M., Costa, E., Garcés, M., Beamud, E., & Larrasoaña, J. C. (2012). Tectonic and climatic controls on the sequential arrangement of an alluvial fan/fan-delta complex (Montserrat, Eocene, Ebro Basin, NE Spain). *Basin Research*, *24*(4), 437–455. <https://doi.org/10.1111/j.1365-2117.2011.00532.x>
- Gutiérrez-Medina, M. (2007). Nuevas aportaciones al conocimiento de la estructura varisca y alpina de la lámina cabalgante de Bono, Zona Axial, Pirineos Centrales. *Trabajos de Geología*, *27*, 159–177.
- Henry, B., Rouvier, H., & Le Goff, M. (2004). Using syntectonic remagnetizations for fold geometry and vertical axis rotation: The example of the Cévennes border (France). *Geophysical Journal International*, *157*(3), 1061–1070. <https://doi.org/10.1111/j.1365-246X.2004.02277.x>
- Institut Cartogràfic i Geològic de Catalunya (2014). Mapa Estructural de Catalunya 1:250.000 Primera Edició.
- Izquierdo-Llavall, E., Aldega, L., Cantarelli, V., Corrado, S., Gil-Peña, I., Invernizzi, C., & Casas, A. M. (2013). On the origin of cleavage in the Central Pyrenees: Structural and paleo-thermal study. *Tectonophysics*, *608*, 303–318. <https://doi.org/10.1016/j.tecto.2013.09.027>
- Izquierdo-Llavall, E., Casas-Sainz, A., & Oliva-Urcia, B. (2013). Heterogeneous deformation recorded by magnetic fabrics in the Pyrenean Axial Zone. *Journal of Structural Geology*, *57*, 97–113. <https://doi.org/10.1016/j.jsg.2013.10.005>
- Izquierdo-Llavall, E., Casas-Sainz, A., Oliva-Urcia, B., & Scholger, R. (2014). Palaeomagnetism and magnetic fabrics of the Late Palaeozoic volcanism in the Castejón-Laspaúles basin (central Pyrenees). Implications for palaeoflow directions and basin configuration. *Geological Magazine*, *1–21*.
- Izquierdo-Llavall, E., Sainz, A. C., Oliva-Urcia, B., Burmester, R., Pueyo, E. L., & Housen, B. (2015). Multi-episodic remagnetization related to deformation in the Pyrenean Internal Sierras. *Geophysical Journal International*, *201*(2), 891–914. <https://doi.org/10.1093/gji/ggv042>
- Koymans, M. R., Langereis, C. G., Pastor-Galan, D., & van Hinsbergen, D. J. J. (2016). Paleomagnetism.org: An online multi-platform open source environment for paleomagnetic data analysis. *Computers and Geosciences*, *93*, 127–137. <https://doi.org/10.1016/j.cageo.2016.05.007>
- Kruiver, P. P., Dekkers, M. J., & Heslop, D. (2001). Quantification of magnetic coercivity by analysis of acquisitions curves of isothermal remanent magnetisation. *Earth and Planetary Science Letters*, *189*(3–4), 269–276. [https://doi.org/10.1016/S0012-821X\(01\)00367-3](https://doi.org/10.1016/S0012-821X(01)00367-3)
- López-Mir, B., Muñoz, J. A., & Senz, J. G. (2014). Restoration of basins driven by extension and salt tectonics: Example from the Cotiella Basin in the central Pyrenees. *Journal of Structural Geology*, *69*, 147–162. <https://doi.org/10.1016/j.jsg.2014.09.022>
- Lowrie, W. (1990). Identification of ferromagnetic minerals in a rock by coercivity and unblocking temperature properties. *Geophysical Research Letters*, *17*, 159–162. <https://doi.org/10.1029/GL017i002p00159>
- Martí, J., & Mitjavila, J. (1987). Calderas volcánicas pasivas: Un ejemplo en el Estefaniense del Pirineo Catalán. *Geogaceta*, *2*, 19–22.
- Martínez-Peña, M. B., & Casas-Sainz, A. M. (2003). Cretaceous-Tertiary tectonic inversion at the Cotiella nappe (southern Pyrenees, Spain). *Geologische Rundschau*, *92*, 99–113.
- McCaig, A. M., & McClelland, E. (1992). Palaeomagnetic techniques applied to thrust belts. In K. R. McClay (Ed.), *Thrust tectonics* (pp. 209–216). London: Chapman and Hall. https://doi.org/10.1007/978-94-011-3066-0_19
- McClay, K., Muñoz, J. A., & García-Senz, J. (2004). Extensional salt tectonics in a contractional orogen: A newly identified tectonic event in the Spanish Pyrenees. *Geology*, *32*(9), 737–740. <https://doi.org/10.1130/G20565.1>
- McClelland, E. A., & McCaig, A. M. (1989a). Palaeomagnetic estimates of rotation in basement thrust sheets, Axial Zone, southern Pyrenees. *Cuadernos de Geología Ibérica*, *12*, 181–193.
- McClelland, E. A., & McCaig, A. M. (1989b). Palaeomagnetic estimates of rotations in compressional regimes and potential discrimination between thin-skinned and deep crustal deformation. In: Palaeomagnetic rotations and continental deformation. *NATO ASI series C*, *254*, 365–379.
- McFadden, P. L., & Jones, D. L. (1981). The fold test in palaeomagnetism. *Geophysical Journal of the Royal Astronomical Society*, *67*(1), 53–58. <https://doi.org/10.1111/j.1365-246X.1981.tb02731.x>

- McFadden, P. L., & McElhinny, M. W. (1990). Classification of the reversal test in palaeomagnetism. *Geophysical Journal International*, 103(3), 725–729. <https://doi.org/10.1111/j.1365-246X.1990.tb05683.x>
- McFadden, P. L., & Reid, A. B. (1982). Analysis of palaeomagnetic inclination data. *Geophysical Journal International*, 69(2), 307–319. <https://doi.org/10.1111/j.1365-246X.1982.tb04950.x>
- Mellere, D., & Marzo, M. (1992). Los depósitos aluviales sintectónicos de la Pobl de Segur: Alogrupos y su significado tectonoestratigráfico. *Acta Geologica Hispánica*, 27, 145–159.
- Mey, P. (1968). The geology of the Upper Ribagorzana and Valiera valleys, central Pyrenees, Spain. *Leidse Geologische Mededelingen*, 41, 153–220.
- Mochales, T., Casas, A. M., Pueyo, E. L., & Barnolas, A. (2012). Rotational velocity for oblique structures (Bolton anticline, southern Pyrenees). *Journal of Structural Geology*, 35, 2–16. <https://doi.org/10.1016/j.jsg.2011.11.009>
- Mouthereau, F., Filleaudeau, P. Y., Vacherat, A., Pik, R., Lacombe, O., Fellin, M. G., et al. (2014). Placing limits to shortening evolution in the Pyrenees: Role of margin architecture and implications for the Iberia/Europe convergence. *Tectonics*, 33, 2283–2314. <https://doi.org/10.1002/2014TC003663>
- Muñoz, J. A. (1992). Evolution of a continental collision belt: ECORS-Pyrenees crustal balanced cross-section. In K. R. McClay (Ed.), *Thrust tectonics* (pp. 235–246). London: Chapman and Hall. https://doi.org/10.1007/978-94-011-3066-0_21
- Muñoz, J. A. (2002). The Pyrenees. Alpine Tectonics I: the alpine system north of the Betic Cordillera. In W. Gibbons & T. Moreno (Eds.), *The geology of Spain* (pp. 370–385). The geological society, London.
- Muñoz, J. A., Beamud, E., Fernández, O., Arbués, P., Dinarès-Turell, J., & Poblet, J. (2013). The Ainsa fold and thrust oblique zone of the central Pyrenees: Kinematics of a curved contractional system from paleomagnetic and structural data. *Tectonics*, 32, 1142–1175. <https://doi.org/10.1002/tect.20070>
- Oliva-Urcia, B., & Pueyo, E. L. (2007). Rotational basement kinematics deduced from remagnetized cover rocks (Internal Sierras, southwestern Pyrenees). *Tectonics*, 26, TC4014. <https://doi.org/10.1029/2006TC001955>
- Oliva-Urcia, B., Pueyo, E. L., Larrasoña, J. C., Casas, A. M., Román-Berdiel, T., Van der Voo, R., & Scholger, R. (2012). New and revisited paleomagnetic data from Permian-Triassic red beds: Two kinematic domains in the west-central Pyrenees. *Tectonophysics*, 522–523, 158–175. <https://doi.org/10.1016/j.tecto.2011.11.023>
- Osete, M. L., & Palencia-Ortas, A. (2006). Polos paleomagnéticos de Iberia de los últimos 300 millones de años. *Física de la Tierra*, 18, 157–181.
- Osete, M. L., Rey, D., Villalain, J. J., & Juárez, M. T. (1997). The Late Carboniferous to Late Triassic segment of the apparent polar wander path of Iberia. *Geologie en Mijnbouw*, 76(1/2), 105–119. <https://doi.org/10.1023/A:1003197500052>
- Parés, J. M., Van der Voo, R., & Stamatakos, J. A. (1996). Paleomagnetism of Permian and Triassic red beds of NW Spain and implications for the tectonic evolution of the Asturian-Cantabrian arc. *Geophysical Journal International*, 126(3), 893–901. <https://doi.org/10.1111/j.1365-246X.1996.tb04711.x>
- Pla, O., Izquierdo-Llavall, E., Roca, E., Muñoz, J. A., Rowan, M., Neng, Y., & Ferrer, O. (2017). Influence of syn-tectonic sedimentary rate on the geometry and kinematic evolution of growing experimental wedges: Comparison to Kuqa fold-and-thrust system (NW China). In *Abstracts book of fold and thrust belts: Structural style, evolution and exploration* (pp. 143–144). London: Geological Society of London.
- Poblet, J. (1991). Estructura de les unitats del vessant sud de la zona axial del Pirineu central, (PhD thesis). Spain: University de Barcelona.
- Pueyo, E. (2000). Rotaciones paleomagnéticas en sistemas de pliegues y cabalgamientos. Tipos, causas, significado y aplicaciones. (Ejemplos de las Sierras Exteriores y Cuenca de Jaca, Pirineo Aragonés), PhD Thesis, Univ. de Zaragoza, Spain.
- Pueyo, E. L., Beamud, E., Muñoz, J. A., Rodríguez-Pintó, A., & San Miguel, G. (2016). Remagnetización alpina en la Serra del Cadí (Pirineo Oriental). *Geotemas*, 16(1), 869–872.
- Pueyo, E. L., Oliva-Urcia, B., Sussman, A. J., & Cifelli, F. (2016). Palaeomagnetism in fold and thrust belts: Use with caution. In E. L. Pueyo, F. Cifelli, A. Sussman, & B. Oliva-Urcia (Eds.), *Palaeomagnetism in fold and thrust belts: New perspectives* (Vol. 425, pp. 259–276). London Special Publication: Geological Society.
- Pueyo, E. L., Pocoví, A., Millán, H., & Sussman, A. (2004). Map-view models for correcting and calculating shortening estimates in rotated thrust fronts using paleomagnetic data, in orogenic curvature: Integrating paleomagnetic and structural analyses, edited by A.J. Sussman and A.B. Weil. *Geological Society of America Special Papers*, 383, 57–71.
- Pueyo-Anchuela, Ó., Pocoví, A., Gil-Imaz, A., & Casas-Sainz, A. M. (2013). Factors influencing magnetic susceptibility in the southern Pyrenees. *Studia Geophysica et Geodaetica*, 57(4), 692–709. <https://doi.org/10.1007/s11200-013-0919-2>
- Puigdefàbregas, C., Muñoz, J. A., & Vergés, J. (1992). Thrusting and foreland basin evolution in the southern Pyrenees. In *Thrust tectonics* (pp. 247–254). Dordrecht: Springer.
- Pulliaiah, G., Irving, E., Buchan, K. L., & Dunlop, D. J. (1975). Magnetization changes caused by burial and uplift. *Earth and Planetary Science Letters*, 28(2), 133–143. [https://doi.org/10.1016/0012-821X\(75\)90221-6](https://doi.org/10.1016/0012-821X(75)90221-6)
- Ramón, M. J., Pueyo, E. L., Oliva-Urcia, B., & Larrasoña, J. C. (2017). Virtual directions in paleomagnetism: A global and rapid approach to evaluate the NRM components. *Frontiers in Earth Science*, 5(8), 1–14.
- Ramón, M. J., Pueyo, E. L., Oliva-Urcia, B., Scholger, R., Román-Berdiel, M. T., & Casas, A. M. (2016). Squeezing paleomagnetic information using virtual directions; an example from the Bielsa granite (Axial Pyrenees). *Geotemas*, 16(1), 873–876.
- Rodríguez-Pintó, A., Pueyo, E. L., Sánchez, E., Calvin, P., Ramajo, J., Ramón, M. J., et al. (2016). Rotational kinematics of a curved fold: A structural and paleomagnetic study in the Balzes anticline (southern Pyrenees). *Tectonophysics*, 677, 171–189. <https://doi.org/10.1016/j.tecto.2016.02.049>
- Román-Berdiel, T., Casas, A. M., Oliva-Urcia, B., Pueyo, E. L., Liesa, C., & Soto, R. (2006). The Variscan Millares granite (central Pyrenees): Pluton emplacement in a T fracture of a dextral shear zone. *Geodinamica Acta*, 19(3–4), 197–211. <https://doi.org/10.3166/ga.19.197-211>
- Román-Berdiel, T., Casas, A. M., Oliva-Urcia, B., Pueyo, E. L., & Rillo, C. (2004). The main Variscan deformation event in the Pyrenees: New data from the structural study of the Bielsa granite. *Journal of Structural Geology*, 4, 659–677.
- Saura, E., & Teixell, A. (2006). Inversion of small basins: Effects on structural variations at the leading edge of the axial zone antiformal stack (southern Pyrenees, Spain). *Journal of Structural Geology*, 28(11), 1909–1920. <https://doi.org/10.1016/j.jsg.2006.06.005>
- Schott, J. J., & Perés, A. (1987). Paleomagnetism of Permo-Triassic red beds from the Asturias and Cantabrian chain (northern Spain): Evidence for strong lower Tertiary remagnetizations. *Tectonophysics*, 140(2–4), 179–191. [https://doi.org/10.1016/0040-1951\(87\)90228-9](https://doi.org/10.1016/0040-1951(87)90228-9)
- Séguret, M. (1972). Etude tectonique des nappes et séries décollées de la partie centrale du versant sud des Pyrénées. Caractère syndémitaire, rôle de la compression et de la gravité. Pub. U.S.T.L., Montpellier. Série Géol. Struc., 2.
- Shipunov, S. V. (1997). Synfolding magnetization: Detection, testing and geological applications. *Geophysical Journal International*, 130(2), 405–410. <https://doi.org/10.1111/j.1365-246X.1997.tb05656.x>
- Sussman, A. J., & Weil, A. B. (2004). Orogenic curvature: Integrating paleomagnetic and structural analyses. *Geological Society of America Special Papers*, 383, 258 pp.

- Taberner, C., Dinarès-Turell, J., Giménez, J., & Docherty, C. (1999). Basin infill architecture and evolution from magnetostratigraphic cross basin correlations in the southeastern Pyrenean foreland basin. *Geological Society of America Bulletin*, *11*, 1155–1174.
- Tan, X., & Kodama, K. P. (2002). Magnetic anisotropy and paleomagnetic inclination shallowing in red beds: Evidence from the Mississippian Mauch Chunk Formation, Pennsylvania. *Journal of Geophysical Research*, *107*(B11), 2311. <https://doi.org/10.1029/2001JB001636>
- Tauxe, L. with contributions from Butler, R. F., Van der Voo, R., & Banerjee, S. K. (2010). *Essentials of paleomagnetism*, University of California Press.
- Teixell, A. (1996). The Ansó transect of the southern Pyrenees: Basement and cover thrust geometries. *Journal of the Geological Society*, *153*(2), 301–310. <https://doi.org/10.1144/gsjgs.153.2.0301>
- Teixell, A. (1998). Crustal structure and orogenic material budget in the west central Pyrenees. *Tectonics*, *17*, 395–406. <https://doi.org/10.1029/98TC00561>
- Teixell, A., Labaume, P., & Lagabrielle, Y. (2016). The crustal evolution of the west-central Pyrenees revisited: Inferences from a new kinematic scenario. *Comptes Rendus Geoscience*, *348*(3–4), 257–267. <https://doi.org/10.1016/j.crte.2015.10.010>
- Verges, J., & Munoz, J. A. (1990). Thrust sequence in the southern central Pyrenees. *Bulletin de la Société Géologique de France*, *6*(2), 265–271.
- Weil, A. B., & Sussman, A. (2004). Classification of curved orogens based on the timing relationships between structural development and vertical axis rotations, in *orogenic curvature: Integrating paleomagnetic and structural analyses*, edited by A. J. Sussman and A. B. Weil. *Special Papers: Geological Society of America*, *383*, 1–17.
- Wennekers, J. H. N. (1968). Geological map of the central Pyrenees 1:50000, sheet 7. (Lys-Caillauas-Esera). IGME.
- Zulauf, G., & Duyster, J. (1997). Supracrustal intraplate thickening of Variscan basement due to Alpine foreland compression: Results from the superdeep well KTB (Bohemian massif, Germany). *Tectonics*, *16*, 730–743. <https://doi.org/10.1029/97TC01656>
- Zwart, H. J. (1979). The geology of the central Pyrenees. *Leidse Geologische Mededelingen*, *50*, 1–44.